Received 13 March 2022; revised 28 June 2022 and 25 August 2022; accepted 2 September 2022. Date of publication 15 September 2022; date of current version 14 October 2022. Recommended by Senior Editor Sonia Martinez.

Digital Object Identifier 10.1109/OJCSYS.2022.3206710

Real Time Li-Ion Battery Bank Parameters Estimation via Universal Adaptive Stabilization

SHAYOK MUKHOPADHYAY [1] (Member, IEEE), HAFIZ M. USMAN [1,2] (Student Member, IEEE), AND HABIBUR REHMAN [1] (Member, IEEE)

[1]Department of Electrical Engineering, American University of Sharjah, Sharjah 26666, UAE
[2]Department of Electrical and Computer Engineering, University of Waterloo, Waterloo, ON N2L 3G1, Canada

CORRESPONDING AUTHOR: SHAYOK MUKHOPADHYAY (e-mail: smukhopadhyay@aus.edu).

This work was supported in part by the Office of Research and Graduate Studies at the American University of Sharjah under Grant FRG17-R-34.

ABSTRACT This paper proposes an accurate and efficient Universal Adaptive Stabilizer (UAS) based online parameters estimation technique for a 400 V Li-ion battery bank. The battery open circuit voltage, parameters modeling the transient response, and series resistance are all estimated in a single real-time test. In contrast to earlier UAS based work on individual battery packs, this work does not require prior offline experimentation or any post-processing. Real time fast convergence of parameters' estimates with minimal experimental effort enables update of battery parameters during run-time. The proposed strategy is mathematically validated and its performance is demonstrated on a 400 V, 6.6 Ah Li-ion battery bank powering an induction motor driven prototype electric vehicle (EV) traction system.

INDEX TERMS Adaptive parameters estimation, battery bank, electric vehicle traction system, Li-ion battery, real-time parameters' estimation, universal adaptive stabilizer.

I. INTRODUCTION

High energy density and low self-discharge rate have made Li-ion batteries a premium candidate for electric vehicle (EV) applications. Accurate estimation of open circuit voltage (OCV), series resistance, and State-of-Charge (SoC) are indispensable for an effective battery management system. Precise estimates of internal states of a Li-ion battery like SoC, State-of-Health (SoH) also rely on an accurate battery model. The Chen and Mora equivalent circuit model [1] has been widely adopted in the literature for Li-ion battery modeling. The salient features of this model are: it can model real time voltage and current dynamics; can capture temperature effects and the effect of the number of charge-discharge cycles; it is simple to implement for a run-time battery management system; has low computational effort, and it includes SoC dependent equivalent circuit elements without requiring to solve partial differential equations (PDEs) common in electrochemical Li-ion battery models. Therefore, Chen and Mora's battery model [1] has been utilized in this work [2], [3], [4]. Different strategies are available in the literature for extracting Li-ion battery model parameters [5], [6], [7], [8], [9], [10], [11], [12], [13], [14], [15], [16].

Dual unscented Kalman filter [5] and H_∞ Kalman filter [6] based approaches were proposed to overcome the limitations of Kalman Filters (KFs) and Extended Kalman Filters (EKFs) for accurate battery SoC estimation. Such methods require prior knowledge of battery model parameters. A fractional calculus based equivalent circuit model of a Li-ion battery is presented in [7]. The authors in [7] use the Particle Swarm Optimization (PSO) algorithm for estimation of equivalent circuit elements. Yet this strategy requires a precise knowledge of open circuit voltage, PSO requires high computational effort, and optimality is not guaranteed as it is heuristic based. The authors in [8] proposed a moving window based least squares method to reduce the complexity and computational cost of online equivalent circuit elements' identification, along with the battery SoC estimation. But, the length of the linear approximation window may affect the overall accuracy. Attempts in [9] were made to identify the equivalent circuit elements of a Li-ion battery model by voltage relaxation tests, this requires several offline pulse charging and discharging experiments, and accurate open circuit voltage measurement. Two extended Kalman filters (named as dual EKF) are combined in [10] for simultaneous estimation of Li-ion battery

model parameters and SoC. However, the accuracy of estimated parameters and open circuit voltage are not analyzed in [10]. More recently, a variable time window-based least squares method in [11] is proposed to effectively capture the nonlinear dynamics of a Li-ion battery. Similarly, a partial adaptive forgetting factor-based least squares method is proposed in [12] for Li-ion battery parameters estimation in electric vehicles. Likewise, a trust region optimization-based least squares approach is proposed in [13], which claims to reduce the complexity, and thus the estimation time, compared to a conventional least squares estimation procedure. To overcome the potential limitations of Genetic Algorithm (GA), such as higher computational effort, and possible convergence to local minima, the authors in [14] deployed the Particle Swarm Optimization (PSO) routine after GA for accurate identification of both temperature and SoC dependent Li-ion battery parameters. An algorithm based on a high pass filter and active current injections is developed in [15] for accurate and quick estimation of Li-ion battery parameters. It is shown in [15] that higher frequencies in an injected current improves the performance of the parameters estimation process. Various Neural Network (NN)-based data-driven strategies have also been reported in the literature for Li-ion battery parameters estimation. Different variants of NN-based methods, such as [16] learn and capture the dynamics of a Li-ion battery model. However, the major downsides of [11], [12], [13], [14] include offline pre-processing for appropriate selection of initial parameters, offline open-circuit voltage determination, appropriate tuning of optimization parameters, higher computational efforts, and unsatisfactory convergence performance. The performance of NN-based methods [16] also relies on effective training with large datasets, requiring extensive time-commitments for testing and data collection.

There is research related to parameters identification of batteries in electric vehicles using adaptive forgetting factors with least squares estimation [17]. However, even [17] requires offline experimentation and analysis for determining the open circuit voltage (OCV). There has been recent work [18] comparing Nelder-Mead particle swarm optimization (NM-PSO) and OCV-recursive least squares (RLS) for battery parameters estimation, although the work [18] still needs OCV determination separately, and the computational time requirements of PSO are high too. Further, the authors in [18] show the computation time, and data requirements for different methods. They show that NN-based, machine learning (ML)-based, and porous electrode theory based methodologies require the most amount of data. Whereas, electrochemical, and even single particle models require substantial amounts of data and computation time. There have been recent efforts related to coming up with SoC dependent Li-ion battery models [19], [20], [21]. However, such efforts use a simplified model of a Li-ion battery with only one time constant, which may be limiting in terms of modeling transient voltage dynamics. Also, [19], [20], [21] require separate experiments for gathering the OCV data, and terminal voltage data. In contrast, eliminating the need to perform multiple experiments, and not having to disconnect the battery from the load periodically and letting the voltage settle for observing the OCV, are the motivations and salient features of the work in this paper. Literature also exists related to the identifiability of Li-ion battery model parameters [22]. As mentioned in [22], if an incorrect model structure is chosen this can hinder identifiability due to observability issues that may arise out of an incorrect choice/assumption about the model structure. Also, even if a satisfactory model structure is available, using black-box estimation may require estimating a large number of parameters, for which it may be challenging to select the type and number of inputs that provide sufficient excitation to the system towards ensuring that parameters can be identified [22]. This in-turn leads to increased number of experiments or increased data and computation time requirements.

A novelty of this work is that a physics based approach is combined with an advanced adaptive technique, specifically to get around the above identifiability issues. Several works in the literature have used equivalent circuit models, which are known to be identifiable. Thus inspired we choose an equivalent circuit model too, but the one chosen has parameters that allow variation of the circuit elements values with change in SoC. To create the proposed UAS-based high-gain adaptive observer, a copy of the same equivalent circuit model is created where the elements values update with the estimation error, and an adaptive control signal forces the observer's states to remain close to the actual internal states. And the chosen strategy has the advantage that the adaptive control input vanishes when the estimation error goes to zero. In other words, the only means now for the time evolution of the estimated states to remain close to the time evolution of the actual states is possible if the parameters themselves have acquired the correct values. If not, the estimated states drift apart from the actual states, and the estimation error increases, which causes a change in the estimated parameters values, and also an increase in the adaptive control signal which now tries to reduce the estimation error. So, effectively the only way to run with zero adaptive control effort requires zero estimation error, which is only possible if the evolution of the estimated and actual states are exactly the same, which further requires the estimated parameters to evolve to be the same as the actual parameters. As shown in this paper, selecting the model parameters bounds and initial values based on other models of Li-ion batteries available in the literature e.g. [1] allows very fast parameters estimation, and with only one experimentation run required. Due to the speed of convergence, it can also be suitable for real-time applications.

This work proposes a UAS-based adaptive parameters estimation scheme for a Li-ion battery that does not need any kind of offline pre-processing. Unlike optimization and NN-based methods, the proposed method is very quick and yet effective. Thus it maybe suitable for BMS and real-time EV applications. The proposed method has been tested and verified at the battery cell, pack, and bank levels for simultaneous estimation of battery parameters, and open circuit voltage. This work utilizes a high-gain universal adaptive stabilization (UAS) based

observer. The switching function required by UAS [23], is realized by a Nussbaum function. A Nussbaum function has rapid oscillations and variable frequency by definition [23]. When a Nussbaum function is input to the observer, it injects enough sinusoids into the high-gain observer, possibly satisfying the required persistence of excitation (PE) condition. Detailed discussion related to this is available in Section VIII-B. The contributions of this work are as follows. This work extends previous work in [2] further, by estimating Li-ion battery open circuit voltage, series resistance and other battery model parameters; all in a single experiment conducted in real-time. The proposed approach is validated at the battery cell, pack levels as well as on a 400 V, 6.6Ah Li-ion battery bank supplying an induction motor driven prototype EV traction system. In our previous work, open circuit voltage and series resistance parameters were found by the voltage relaxation test and curve fitting, respectively, and then the remaining parameters were estimated using a UAS based strategy. The previous offline adaptive parameters estimation (APE) strategy in [2] required eight experiments to estimate all battery model parameters, while the proposed online APE scheme runs online requiring only one experiment for parameters estimation. Furthermore, in contrast to [5], [6], [7], [8], [9], [10], our proposed strategy does not require any prior experimentation to gain knowledge of the open circuit voltage, rather the open circuit voltage is also estimated by the strategy proposed in this paper. Compared to previous work, the current work also shows by derivations that all the state and parameters estimates converge to their actual values. And in addition to presenting the conditions required to be checked to ensure such convergence occurs, this work also provides the conditions that the choices of initial values, upper and lower bounds must satisfy to get convergence.

The rest of the article is organized as follows. Necessary background information about the CM [1] Li-ion battery equivalent circuit model and UAS are provided in Section II. Section III formulates the proposed UAS based high gain adaptive observer for parameters estimation. Section IV provides mathematical justification of our proposed method. Simulation and experimental results are presented in Section V and VI respectively for validating the proposed online APE strategy. Real time implementation results for an EV traction system are shared in Section VII. A discussion related to the PE condition, selection of bounds, initial guesses and confidence levels required for the proposed approach, and Li-ion battery stability, is available in Section VIII. Finally, the concluding remarks are made in Section IX of this article.

II. BACKGROUND

This section provides information about the CM Li-ion battery equivalent circuit model and UAS used in this work. The battery equivalent circuit model is described in Section II-A, while Section II-B presents the details of the Nussbaum type switching function employed in the proposed online APE algorithm.

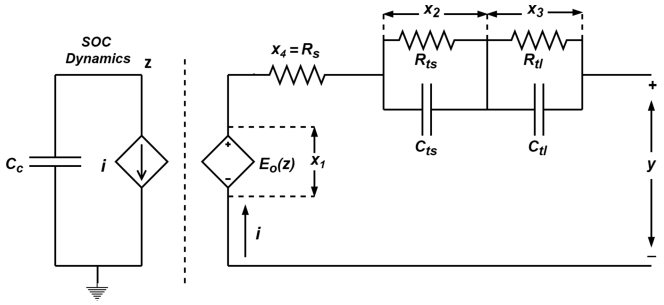

FIGURE 1. Li-ion battery equivalent circuit model.

A. LI-ION BATTERY EQUIVALENT CIRCUIT MODEL

The Chen and Mora [1] equivalent circuit model of a Li-ion battery is shown in Fig. 1. This work aims at providing an accurate and simple online adaptive parameters estimation method, for a battery at the cell/pack/bank level using the Li-ion battery model shown in Fig. 1. The state space representation of Fig. 1 is described by (1)–(6). Here, the battery SoC is denoted by $z \in [0, 1]$. The discharge current $i(t) \geq 0$. The states x_1, x_2, x_3, x_4, represent the open circuit voltage, the voltage across $R_{ts}||C_{ts}$, the voltage across $R_{tl}||C_{tl}$, and the battery series resistance R_s respectively. The term C_c and $y(t)$ denote the battery capacity in ampere-hour (Ah) and battery terminal voltage. The factors f_1, f_2, $f_3 \in [0, 1]$ account for the effects of temperature, charge-discharge cycles, and self discharging respectively. The battery open circuit voltage x_1 in (2), battery series resistance x_4 in (5), and equivalent circuit elements $R_{ts}, R_{tl}, C_{ts}, C_{tl}$ can be defined from Chen and Mora's work [1] by (7)–(12). Note that the formulation in (1)–(5) is novel compared to [2], as the notation introduced here for the CM model specifically allows simultaneous online estimation of battery parameters, and open circuit voltage.

$$\dot{z}(t) = -\frac{1}{C_c} i(t),\ C_c = 3600 C f_1 f_2 f_3,$$
$$z(t_0) = z_0, 0 \leq z_0 \leq 1$$
$$\dot{x}_1(t) = \frac{\partial x_1(z)}{\partial z(t)} \dot{z}(t),\ \text{therefore} \tag{1}$$
$$\dot{x}_1(t) = -\left(r_1 r_2 e^{-r_2 z} + r_4 - 2 r_5 z + 3 r_6 z^2\right) \frac{i(t)}{C_c} \tag{2}$$
$$\dot{x}_2(t) = -\frac{x_2(t)}{R_{ts}(z) C_{ts}(z)} + \frac{i(t)}{C_{ts}(z)} \tag{3}$$
$$\dot{x}_3(t) = -\frac{x_3(t)}{R_{tl}(z) C_{tl}(z)} + \frac{i(t)}{C_{tl}(z)} \tag{4}$$
$$\dot{x}_4(t) = \frac{\partial x_4(z(t))}{\partial z(t)} \dot{z}(t) = \left(r_{19} r_{20} e^{-r_{20} z}\right) \frac{i(t)}{C_c} \tag{5}$$
$$y(t) = x_1(z) - x_2(t) - x_3(t) - i(t) x_4(t). \tag{6}$$
$$E_o(z) = -r_1 e^{-r_2 z} + r_3 + r_4 z - r_5 z^2 + r_6 z^3 = x_1(z) \tag{7}$$
$$R_{ts}(z) = r_7 e^{-r_8 z} + r_9 \tag{8}$$

$$R_{tl}(z) = r_{10}e^{-r_{11}z} + r_{12} \tag{9}$$

$$C_{ts}(z) = -r_{13}e^{-r_{14}z} + r_{15} \tag{10}$$

$$C_{tl}(z) = -r_{16}e^{-r_{17}z} + r_{18} \tag{11}$$

$$R_s(z) = r_{19}e^{-r_{20}z} + r_{21} = x_4(z). \tag{12}$$

The parameters $r_1, \ldots, r_{21}$ used in the circuit elements in equation (7)–(12) are all constant positive real numbers.

B. UNIVERSAL ADAPTIVE STABILIZATION

The UAS based strategy has been employed in [24] for fast error convergence. This motivated us to employ the UAS based adaptive estimation method for quick [24] and yet accurate [2], [4], [25] Li-ion battery parameters $(r_1, \ldots, r_{21})$ estimation. The implementation of a UAS based technique requires a switching function with high growth rate [23]. A Nussbaum function is a switching function, which is defined as a piecewise right continuous function $N(\cdot) : [k', \infty) \to \mathbb{R}$, $k_0 > k'$, that satisfies (13) and (14).

$$\sup_{k>k_0} \frac{1}{k-k_0} \int_{k_0}^{k} N(\tau)d\tau = +\infty, \tag{13}$$

$$\inf_{k>k_0} \frac{1}{k-k_0} \int_{k_0}^{k} N(\tau)d\tau = -\infty. \tag{14}$$

Here, $k_o \in (k', \infty)$. In this work a Nussbaum type switching function has been implemented using the Mittag-Leffler (ML) function, described by (15).

$$E_\alpha(\rho) = \sum_{k=0}^{\infty} \frac{\rho^k}{\Gamma(k\alpha + 1)}, \tag{15}$$

Here $\Gamma(\rho + 1) = \rho\Gamma(\rho)$, $\rho > 0$ is the standard Gamma function. A Nussbaum switching function of ML type is employed in this work and in [2], [4] for the UAS based adaptation strategy. If $\alpha \in (2, 3]$ and $\lambda > 0$ then the ML function $E_\alpha(-\lambda t^\alpha)$ is a Nussbaum function [26]. The MATLAB implementation of an ML type Nussbaum switching function can be found in [27]. In the section III, a proposed UAS observer-based Li-ion battery model parameter estimator is described for accurate estimation of battery model parameters $r_1, \ldots, r_{21}$.

III. PROPOSED ADAPTIVE PARAMETERS ESTIMATION METHODOLOGY OF A LI-ION BATTERY MODEL

This first subsection provides the formulation details, whereas, the second section describes the operational flow of our proposed methodology.

A. PROPOSED UAS BASED BATTERY PARAMETERS ESTIMATION METHODOLOGY

A high gain adaptive estimator for a Li-ion battery model, based on (1)–(6), is described by (16)–(21).

$$\dot{\hat{z}}(t) = -\frac{1}{C_c} i(t), C_c = 3600Cf_1f_2f_3, \ \hat{z}(t_0) = z(t_0)$$

$\dot{\hat{x}}_1(t) = \frac{\partial \hat{x}_1(\hat{z})}{\partial \hat{z}(t)} \dot{\hat{z}}(t) - u(t), \hat{x}_1(t) \geq 0$, therefore giving (16)

$$\dot{\hat{x}}_1(t) = -\left(\hat{r}_1\hat{r}_2 e^{-\hat{r}_2\hat{z}} + \hat{r}_4 - 2\hat{r}_5\hat{z} + 3\hat{r}_6\hat{z}^2\right)\frac{i(t)}{C_c} - u(t), \tag{17}$$

$$\dot{\hat{x}}_2(t) = -\frac{\hat{x}_2(t)}{\hat{R}_{ts}(\hat{z})\hat{C}_{ts}(\hat{z})} + \frac{i(t)}{\hat{C}_{ts}(\hat{z})} + u(t), \quad \hat{x}_2(t) \geq 0 \tag{18}$$

$$\dot{\hat{x}}_3(t) = -\frac{\hat{x}_3(t)}{\hat{R}_{tl}(\hat{z})\hat{C}_{tl}(\hat{z})} + \frac{i(t)}{\hat{C}_{tl}(\hat{z})} + u(t), \quad \hat{x}_3(t) \geq 0 \tag{19}$$

$\dot{\hat{x}}_4(t) = \frac{\partial \hat{x}_4(\hat{z}(t))}{\partial \hat{z}(t)} \dot{\hat{z}}(t) + u(t)$, therefore giving

$$\dot{\hat{x}}_4(t) = \left(\hat{r}_{19}\hat{r}_{20}e^{-\hat{r}_{20}\hat{z}}\right)\frac{i(t)}{C_c} + u(t), \quad \hat{x}_4(t) \geq 0 \tag{20}$$

$$\hat{y}(t) = \hat{x}_1(t) - \hat{x}_2(t) - \hat{x}_3(t) - i(t)\hat{x}_4(t). \tag{21}$$

Here $u(t)$ is the input received from the UAS based observer, $i(t)$ is the actual battery current and $\hat{z}(t)$ is the estimated SoC, which is the same as $z(t)$ in (1). The states $\hat{x}_1$, $\hat{x}_2$, $\hat{x}_3$, and $\hat{x}_4$ denote the estimates of open circuit voltage, voltage across $\hat{R}_{ts}||\hat{C}_{ts}$, $\hat{R}_{tl}||\hat{C}_{tl}$, and estimated series resistance respectively. For simplicity, the values of f_1, f_2, f_3 are taken as 1 in this work. The estimated voltage is represented by $\hat{y}(t)$, whereas the estimated circuit elements are given by (22)–(27).

$$\hat{E}_o(\hat{z}) = -\hat{r}_1 e^{-\hat{r}_2\hat{z}} + \hat{r}_3 + \hat{r}_4\hat{z} - \hat{r}_5\hat{z}^2 + \hat{r}_6\hat{z}^3 = \hat{x}_1(\hat{z}) \tag{22}$$

$$\hat{R}_{ts}(\hat{z}) = \hat{r}_7 e^{-\hat{r}_8\hat{z}} + \hat{r}_9 \tag{23}$$

$$\hat{R}_{tl}(\hat{z}) = \hat{r}_{10} e^{-\hat{r}_{11}\hat{z}} + \hat{r}_{12} \tag{24}$$

$$\hat{C}_{ts}(\hat{z}) = -\hat{r}_{13} e^{-\hat{r}_{14}\hat{z}} + \hat{r}_{15} \tag{25}$$

$$\hat{C}_{tl}(\hat{z}) = -\hat{r}_{16} e^{-\hat{r}_{17}\hat{z}} + \hat{r}_{18} \tag{26}$$

$$\hat{R}_s(\hat{z}) = \hat{r}_{19} e^{-\hat{r}_{20}\hat{z}} + \hat{r}_{21} = \hat{x}_4(\hat{z}). \tag{27}$$

The control input $u(t)$ of the UAS based-observer is designed by employing (28)–(31).

$$e(t) = y(t) - \hat{y}(t), \tag{28}$$

$$\dot{k}(t) = e^2(t), \quad k(t_0) = k_0 \tag{29}$$

$$N(k(t)) = E_\alpha(-\lambda k(t)^\alpha), \tag{30}$$

$$u(t) = -N(k(t))e(t). \tag{31}$$

In this work, the value of $\alpha = 2.5$, and $\lambda = 1$. The adaptive equation for battery parameters estimation from [2], [4], is given by (32).

$$\dot{\hat{r}}_n(t) = e^2(t) + \lambda_{x_n}(r_{n_u} - \hat{r}_n(t)) + \lambda_{y_n}(r_{n_l} - \hat{r}_n(t)). \tag{32}$$

The adaptive update law in (32) requires a steady-state upper bound r_{n_u} and a lower bound r_{n_l} for each estimated parameter $\hat{r}_n(t), n \in \{1, 2, \ldots, 21\}\backslash\{3, 21\}$, and user's confidence levels, λ_{x_n} and λ_{y_n}, on the upper and lower bounds respectively.

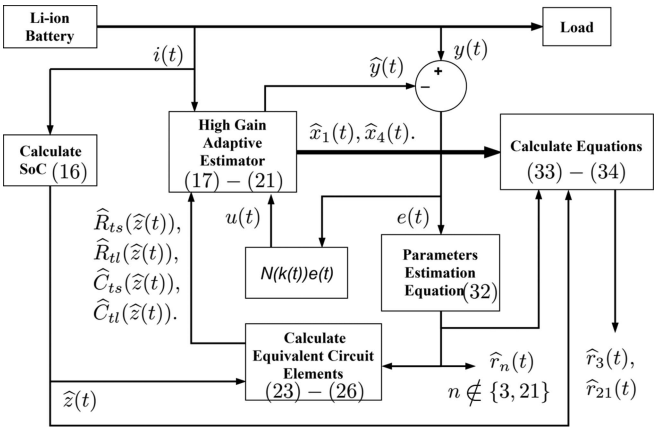

FIGURE 2. Flowchart of the proposed online UAS based adaptive parameters estimation algorithm for Li-ion battery cells/packs/banks.

It is shown in Lemma 2 that $\widehat{r}_n(t)$ converges to a constant with time. Also from (61) it is easy to see that positive real values of $\widehat{r}_n(t_0)$, r_{n_u}, r_{n_l}, λ_{x_n}, and λ_{y_n} lead to $\widehat{r}_n(t) > 0$, for all $t \geq t_0$. The flowchart of the proposed online APE method for Li-ion battery parameters estimation is shown in Fig. 2. Note that the UAS based parameters estimation method, explained above, is capable of estimating the battery parameters $n \in \{1, 2, \ldots, 21\}\backslash\{3, 21\}$. The estimates of $\widehat{r}_3$ and $\widehat{r}_{21}$ can be obtained, during or after the adaptation process, by applying the least squares estimation or curve fitting techniques on (22) and (27) respectively. However, this work uses a direct approach to estimate $\widehat{r}_3$ and $\widehat{r}_{21}$, during the adaptation process. Our approach to estimate $\widehat{r}_3$ and $\widehat{r}_{21}$ is based on the results of Theorem 2. Theorem 2 shows that $\widehat{x}_1(t) \to x_1(t)$ and $\widehat{x}_4(t) \to x_4(t)$, and $\widehat{r}_n \to r_n$ as $t \to \infty$, here $n \in \{1, 2, \ldots, 21\}\backslash\{3, 21\}$. Thus using $\widehat{x}_1(t) \to x_1(t)$ and $\widehat{x}_4(t) \to x_4(t)$ at $t \to \infty$, lets us write the (22) and (27) into the forms shown in (33) and (34) to estimate $\widehat{r}_3$ and $\widehat{r}_{21}$ respectively.

$$\widehat{r}_3 = x_1(t) + \widehat{r}_1 e^{-\widehat{r}_2\widehat{z}} - \widehat{r}_4\widehat{z} + \widehat{r}_5\widehat{z}^2 - \widehat{r}_6\widehat{z}^3, \tag{33}$$

$$\widehat{r}_{21} = x_4(t) - \widehat{r}_{19} e^{-\widehat{r}_{20}\widehat{z}}. \tag{34}$$

The steps to implement the proposed UAS based adaptation methodology for battery model parameters estimation are described next.

B. PROPOSED ALGORITHM FOR ON-LINE LI-ION BATTERY MODEL PARAMETERS ESTIMATION

This section provides the details of our proposed UAS based adaptation algorithm to estimate Li-ion battery model parameters. The flowchart of the algorithm is shown in Fig. 2. The UAS based adaptation process begins with the measurement of current and voltage of a Li-ion battery. As per Theorem 2, a bounded discharge current, with bounded first derivative needs to be maintained during the adaptation, and the current needs to go to zero at some point of time for accurate results. These requirements are not hard to maintain as the discharge current and the rate of change of discharge current are bounded in reality, and also any battery supplying a load will at some point either be shut off, or will die - thus the current will have an opportunity to go to zero even if the profile of the discharge current does not frequently provide opportunities for the current to go to zero. The error between actual and estimated terminal voltages is used by UAS and the adaptive estimation equation in (32) to identify $\widehat{r}_n(t)$, where $n \in \{1, 2, \ldots, 21\}\backslash\{3, 21\}$. These estimated parameters are employed to calculate the equivalent circuit elements. Next, the equivalent circuit elements' estimates, together with the output of UAS and current are input to the high gain adaptive estimator. The adaptation process ends with estimation of the states $\widehat{x}_1(\widehat{t})$, $\widehat{x}_2(t)$, $\widehat{x}_3(t)$, $\widehat{x}_4(\widehat{t})$, followed by terminal voltage estimation error update defined by (28). When the error magnitude goes below the user's defined threshold during the adaptation, the estimated states approach to actual states of a Li-ion battery model, as per Theorem 2. Thereafter, the convergence of estimated states to their actual values allows us to use equation (33) and (34) for identification of $\widehat{r}_3(t)$ and $\widehat{r}_{21}(t)$. In the following section, we provide mathematical justification of our proposed online UAS based adaptation strategy for Li-ion battery model parameters estimation.

IV. MATHEMATICAL JUSTIFICATION

This section first proves the convergence of the terminal voltage estimation error $e(t)$ to zero. Further analysis leads to the conclusion that the proposed method can accurately estimate the Li-ion battery model parameters. Before proving the above results, some criteria for λ_{x_n}, λ_{y_n}, r_{n_u}, and r_{n_l} selection needs to be established in Lemma 1.

Lemma 1: Suppose λ_{x_n}, λ_{y_n}, r_{n_u}, and r_{n_l} are positive real numbers for $n = \{13, 15, 16, 18\}$, and $\widehat{z}(t) \in (0, 1]$, then the following conditions hold for all $t > t_0$. **(i) If** $\widehat{r}_{13}(t_0) > \widehat{r}_{15}(t_0) > 0$, $\lambda_{x_{15}} + \lambda_{y_{15}} > \lambda_{x_{13}} + \lambda_{y_{13}}$, $\lambda_{x_{15}} r_{15_u} + \lambda_{y_{15}} r_{15_l} < \lambda_{x_{13}} r_{13_u} + \lambda_{y_{13}} r_{13_l}$, and $\widehat{r}_{14}(t) > -\dfrac{1}{\widehat{z}(t)} \ln\left(\dfrac{\widehat{r}_{15}(t)}{\widehat{r}_{13}(t)}\right)$, **then** $\widehat{C}_{ts}(\widehat{z}(t)) > 0$. **(ii) If** $\widehat{r}_{16}(t_0) > \widehat{r}_{18}(t_0) > 0$, $\lambda_{x_{18}} + \lambda_{y_{18}} > \lambda_{x_{16}} + \lambda_{y_{16}}$, $\lambda_{x_{18}} r_{18_u} + \lambda_{y_{18}} r_{18_l} < \lambda_{x_{16}} r_{16_u} + \lambda_{y_{16}} r_{16_l}$, and $\widehat{r}_{17}(t) > -\dfrac{1}{\widehat{z}(t)} \ln\left(\dfrac{\widehat{r}_{18}(t)}{\widehat{r}_{16}(t)}\right)$ **then** $\widehat{C}_{tl}(\widehat{z}(t)) > 0$.

Proof: The detailed proof of Lemma 1 is available in [2], Lemma 4.1]. The only notational replacements required are: replace $\widehat{a}, a, \widehat{x}_1$ in [2], Lemma 4.1] by $\widehat{r}, r, \widehat{z}$ respectively to get the required proof. □

For all Li-ion batteries there is a minimum value of the SoC $z_{\min}$ beyond which the battery is not operated. Similarly given any particular fully charged battery there exists a time T beyond which the battery will not be usable i.e. it will be out of charge and will not supply any current. Based on this understanding, it is possible to establish guarantees that allow the conditions $\widehat{r}_{14}(t) > -\dfrac{1}{\widehat{z}(t)} \ln\left(\dfrac{\widehat{r}_{15}(t)}{\widehat{r}_{13}(t)}\right)$ and $\widehat{r}_{17}(t) > -\dfrac{1}{\widehat{z}(t)} \ln\left(\dfrac{\widehat{r}_{18}(t)}{\widehat{r}_{16}(t)}\right)$ to be satisfied for Lemma 1 to hold. This is shown in Corollary 1.

Corollary 1: Given that α, $z_{\min}$, T, a_{min^1}, a_{min^2}, $\lambda_{x_n}, \lambda_{y_n}, r_{n_u}, r_{n_l}$ are positive real numbers, where $n = \{13, 14, 15, 16, 17, 18\}$, $\widehat{z}(t) \in [z_{\min}, 1]$, $T > t_0$. Let $t \in [t_0, T]$, $\alpha > 1, z_{\min} \in (0, 1)$ and assuming $a_{min^1} = \min_{t\in[t_0,T]} \dfrac{\widehat{r}_{15}(t)}{\widehat{r}_{13}(t)}$, $a_{min^2} = \min_{t\in[t_0,T]} \dfrac{\widehat{r}_{18}(t)}{\widehat{r}_{16}(t)}$ exist. Then the following hold:

i) If $\widehat{r}_{13}(t_0) > \widehat{r}_{15}(t_0) > 0$, $\lambda_{x_{15}} + \lambda_{y_{15}} > \lambda_{x_{13}} + \lambda_{y_{13}}$, $\lambda_{x_{15}} r_{15_u} + \lambda_{y_{15}} r_{15_l} < \lambda_{x_{13}} r_{13_u} + \lambda_{y_{13}} r_{13_l}$, $\lambda_{x_{14}} + \lambda_{y_{14}} = \dfrac{1}{T}$, and $\widehat{r}_{14}(t_0) \geq -\alpha e \dfrac{\ln(a_{min^1})}{z_{\min}}$ **then** $\widehat{r}_{14}(t) > -\dfrac{1}{\widehat{z}(t)} \ln\left(\dfrac{\widehat{r}_{15}(t)}{\widehat{r}_{13}(t)}\right)$, for $t \in [t_0, T]$.

ii) If $\widehat{r}_{16}(t_0) > \widehat{r}_{18}(t_0) > 0$, $\lambda_{x_{18}} + \lambda_{y_{18}} > \lambda_{x_{16}} + \lambda_{y_{16}}$, $\lambda_{x_{18}} r_{18_u} + \lambda_{y_{18}} r_{18_l} < \lambda_{x_{16}} r_{16_u} + \lambda_{y_{16}} r_{16_l}$, $\lambda_{x_{17}} + \lambda_{y_{17}} = \dfrac{1}{T}$, and $\widehat{r}_{17}(t_0) \geq -\alpha e \dfrac{\ln(a_{min^2})}{z_{\min}}$, **then** $\widehat{r}_{17}(t) > \ln\left(\dfrac{\widehat{r}_{18}(t)}{\widehat{r}_{16}(t)}\right)$, for $t \in [t_0, T]$.

Proof: Let $T > 0, \alpha > 1, z_{\min} \in (0, 1)$ be given. Suppose $\widehat{r}_{13}(t_0) > \widehat{r}_{15}(t_0) > 0$, $\lambda_{x_{15}} + \lambda_{y_{15}} > \lambda_{x_{13}} + \lambda_{y_{13}}$, $\lambda_{x_{15}} r_{15_u} + \lambda_{y_{15}} r_{15_l} < \lambda_{x_{13}} r_{13_u} + \lambda_{y_{13}} r_{13_l}$, $\lambda_{x_{14}} + \lambda_{y_{14}} = \dfrac{1}{T}$, as per assumptions for proving the first item in the statement of corollary 1. Pick positive real numbers $\lambda_{x_{14}}, \lambda_{y_{14}}$ so that $\lambda_{x_{14}} + \lambda_{y_{14}} = \dfrac{1}{T}$. Pick $\widehat{r}_{14}(t_0) \geq -\alpha e \dfrac{\ln(a_{min^1})}{z_{\min}}$. Based on the assumptions, and by making the following notational replacements i.e. replace $\widehat{a}, a, \widehat{x}_1$ in [2, Lemma 4.1] by $\widehat{r}, r, \widehat{z}$ respectively, and by following the steps in [2, Lemma 4.1] gives $\widehat{r}_{15}(t) < \widehat{r}_{13}(t)$ for all $t > t_0$, $\widehat{r}_{15}(t), \widehat{r}_{13}(t)$ are positive. This provides that $0 < \frac{\widehat{r}_{15}(t)}{\widehat{r}_{13}(t)} < 1$ for all $t > t_0$. And because it is assumed that $a_{min^1} = \min_{t\in[t_0,T]} \dfrac{\widehat{r}_{15}(t)}{\widehat{r}_{13}(t)}$ exists, this provides $0 < a_{min^1} < 1$. Now, the solution to (32) is

$$\begin{aligned}\widehat{r}_{14}(t) = \widehat{r}_{14}(t_0) e^{-(\lambda_{x_{14}}+\lambda_{y_{14}})t} \\ + \left((\lambda_{x_{14}} r_{14_u} + \lambda_{y_{14}} r_{14_l}) \times \int_{t_0}^{t} e^{-(\lambda_{x_{14}}+\lambda_{y_{14}})\tau} d\tau\right) \\ + \int_{t_0}^{t} e^2 (t-\tau) e^{-(\lambda_{x_{14}}+\lambda_{y_{14}})\tau} d\tau. \qquad (35)\end{aligned}$$

From our choice of $\widehat{r}_{14}(t_0)$ we get

$$\begin{aligned}\widehat{r}_{14}(t) \geq -\alpha \frac{\ln(a_{min^1})}{z_{\min}} e^{(1-\frac{t}{T})} \\ + \left((\lambda_{x_{14}} r_{14_u} + \lambda_{y_{14}} r_{14_l}) \times \int_{t_0}^{t} e^{-(\lambda_{x_{14}}+\lambda_{y_{14}})\tau} d\tau\right) \\ + \int_{t_0}^{t} e^2 (t-\tau) e^{-(\lambda_{x_{14}}+\lambda_{y_{14}})\tau} d\tau \qquad (36)\end{aligned}$$

Based on the above discussion, it is easy to see that all terms on the R.H.S. of (36) are positive. Further from the definition of a_{min^1} and because $z_{\min} \in (0, 1), \widehat{z}(t) \in [z_{\min}, 1]$ we get $-\alpha \dfrac{\ln(a_{min^1})}{z_{\min}} e^{(1-\frac{t}{T})} > -\dfrac{1}{\widehat{z}(t)} \ln\left(\dfrac{\widehat{r}_{15}(t)}{\widehat{r}_{13}(t)}\right)$, for $t \in [t_0, T]$. This combined with the fact that that all terms on the R.H.S. of (36) are positive gives $\widehat{r}_{14}(t) > -\dfrac{1}{\widehat{z}(t)} \ln\left(\dfrac{\widehat{r}_{15}(t)}{\widehat{r}_{13}(t)}\right)$, for $t \in [t_0, T]$. This completes the proof of the first statement. For the proof of the second statement, the above process is to be followed by replacing $\widehat{r}_{13}, \widehat{r}_{14}, \widehat{r}_{15}, \lambda_{x_{13}}, \lambda_{x_{14}}, \lambda_{x_{15}}, \lambda_{y_{13}}, \lambda_{y_{14}}, \lambda_{y_{15}}, r_{13_u}, r_{14_u}, r_{15_u}, r_{13_l}, r_{14_l}, r_{15_l}$, and a_{min^1} with $\widehat{r}_{16}, \widehat{r}_{17}, \widehat{r}_{18}, \lambda_{x_{16}}, \lambda_{x_{17}}, \lambda_{x_{18}}, \lambda_{y_{16}}, \lambda_{y_{17}}, \lambda_{y_{18}}, r_{16_u}, r_{17_u}, r_{18_u}, r_{16_l}, r_{17_l}, r_{18_l}$ and a_{min^2} respectively.

The following result shows that the two quantities a_{min^1}, a_{min^2} exist. The existence of these quantities guarantees that the selection of initial values for the parameters estimates which meet the assumptions in Lemma 1, are possible. □

Corollary 2: Given that $\widehat{r}_n(t_0), \lambda_{xn}, \lambda_{yn}, r_{n_u}$ and r_{n_l} are positive real numbers for $n \in \{13, 15, 16, 18\}$, and time $t \in [t_0, T]$, then the quantities $a_{min^1} = \min_{t\in[t_0,T]} \dfrac{\widehat{r}_{15}(t)}{\widehat{r}_{13}(t)}$, $a_{min^2} = \min_{t\in[t_0,T]} \dfrac{\widehat{r}_{18}(t)}{\widehat{r}_{16}(t)}$ exist.

Proof: The solution to (32) provides $\widehat{r}_n(t)$ as shown in (61). From (61), and from assumptions it is obvious that $\widehat{r}_n(t) \neq 0$ for all $t \in [t_0, T]$. Further, all the terms on the R.H.S. of (61) represent continuous functions in time. For this proof, $t \in [t_0, T]$ and $\widehat{r}_n(t) : [t_0, T] \to \mathbb{R}$. So for all $n \in \{13, 15, 16, 18\}$ we have that $\widehat{r}_n(t)$ are continuous functions, on a non-empty compact metric space (please see Theorem 3). Further, let $g_1(t) = \dfrac{\widehat{r}_{15}(t)}{\widehat{r}_{13}(t)}, g_2(t) = \dfrac{\widehat{r}_{18}(t)}{\widehat{r}_{16}(t)}$. From the above discussion we know that $\widehat{r}_{13}(t), \widehat{r}_{18}(t) \neq 0$ for all $t \in [t_0, T]$, and so using Proposition 1 we know that $g_1(t), g_2(t)$ are also continuous. Then, on further application of Corollary 3 we get that $a_{min^1} = \min_{t\in[t_0,T]} g_1(t) = \min_{t\in[t_0,T]} \dfrac{\widehat{r}_{15}(t)}{\widehat{r}_{13}(t)}$, $a_{min^2} = \min_{t\in[t_0,T]} g_2(t) = \min_{t\in[t_0,T]} \dfrac{\widehat{r}_{18}(t)}{\widehat{r}_{16}(t)}$ exist. This completes the proof.

Corollary 2 shows that the quantities a_{min^1} and a_{min^2} exist. Also, Corollary 1 shows that the conditions required for Lemma 1 to hold can be satisfied by simply choosing initial values, upper and lower bounds on the parameters being estimated. This is also not necessarily challenging, because the current work aims to contribute to physics-based system identification, where the user engaging in system identification is expected to have at least a vague idea of the magnitude and the expected range of the physical model parameters that are being estimated, and two positive constants $\alpha, z_{\min}$. The constant α can be chosen to be any number greater than 1, and similarly $z_{\min}$ can be selected as the limit below which the battery SoC is not allowed to fall, e.g. in most cases this limit is around 10% as allowing the battery SoC to fall substantially below this may cause damage to a battery. Further notice that the type of parameters estimation being dealt with in this work is contrary to black-box parameters estimation where the user may have no clue about the model parameters or in some cases even have no idea about the model structure. So for the type of system identification where this work contributes, it is not

unreasonable to request the initial values/guesses, upper and lower bounds on the parameters values from the user. The advantages of this have been mentioned in the introduction, and are also emphasized in the Appendix where the computation time of different parameters estimation strategies are compared.

Further, the conditions established in Lemma 1 are utilized in the following theorem to prove the convergence of terminal voltage error $e(t)$ to zero, which leads to the convergence of estimated values of the circuit elements to actual ones.

Remark 1: The novelty of the mathematical development presented in this work in comparison to the earlier work [2] is the following. In [2], the battery series resistance and battery open circuit voltage are not included as states in the observer. As a result, in [2] parameters related to the battery series resistance and battery open circuit voltage cannot be estimated online but needs pre/post processing of data. In the current work, not only are the battery series resistance and battery open circuit voltage included as states in the proposed observer, but also the parameters $\widehat{r}_1, \ldots, \widehat{r}_6$ of the open circuit voltage in (22) and parameters $\widehat{r}_{19}, \ldots, \widehat{r}_{21}$ of the battery series resistance, in (27) are estimated online. This requires introducing additional states in the proposed observer formulation, and makes the mathematics in this work, much more involved compared to [2].

Theorem 1: Let $i(t) \geq 0$ represent the Li-ion battery discharge current, and let $\widehat{r}_n(t_0) > 0$ for $n \in \{1, 2, \ldots, 21\}\backslash\{3, 21\}$. Further let $y(t)$ be the Li-ion battery voltage as in (6), let $\widehat{y}(t)$ be the estimated terminal voltage as in (21), and let $e(t) = y(t) - \widehat{y}(t)$. **If** the conditions needed for Lemma 1 to hold are satisfied, **then** $e(t) \to 0$ as $t \to \infty$.

Proof: Suppose the assumptions mentioned above are satisfied. Take the time derivative of (28) to get

$$\dot{e}(t) = \dot{y}(t) - \dot{\widehat{y}}(t), \tag{37}$$

Addition and subtraction of $e(t)$ to the R.H.S. of (37), and recognizing that $e(t) = y(t) - \widehat{y}(t)$ provides

$$\dot{e}(t) = -e(t) + y(t) - \widehat{y}(t) + \dot{y}(t) - \dot{\widehat{y}}(t). \tag{38}$$

Now, substitution of $-\widehat{y}(t)$ and $\dot{\widehat{y}}(t)$ from (21) in (38) provides

$$\begin{aligned}\dot{e}(t) = & -e(t) + y(t) + \dot{y}(t) - \widehat{x}_1(\widehat{z}(t)) + \widehat{x}_2(t) + \widehat{x}_3(t) \\ & + i(t)\widehat{x}_4(\widehat{z}(t)) - \dot{\widehat{x}}_1(\widehat{z}(t)) + \dot{\widehat{x}}_2(t) + \dot{\widehat{x}}_3(t) \\ & + \frac{di(t)}{dt}\widehat{x}_4(\widehat{z}(t)) + i(t)\dot{\widehat{x}}_4(\widehat{z}(t))\end{aligned} \tag{39}$$

Using (18) and (19) in (39) gives

$$\begin{aligned}\dot{e}(t) = & -e(t) + y(t) + \dot{y}(t) - \widehat{x}_1(\widehat{z}(t)) + \widehat{x}_2(t) + \widehat{x}_3(t) \\ & + i(t)\widehat{x}_4(\widehat{z}(t)) - \dot{\widehat{x}}_1(\widehat{z}(t)) - \frac{\widehat{x}_2(t)}{\widehat{R}_{ts}(\widehat{z}(t))\widehat{C}_{ts}(\widehat{z}(t))} \\ & - \frac{\widehat{x}_3(t)}{\widehat{R}_{tl}(\widehat{z}(t))\widehat{C}_{tl}(\widehat{z}(t))} + \frac{i(t)}{\widehat{C}_{ts}(\widehat{z}(t))} + \frac{i(t)}{\widehat{C}_{tl}(\widehat{z}(t))} \\ & + 2u(t) + \frac{di(t)}{dt}\widehat{x}_4(\widehat{z}(t)) + i(t)\dot{\widehat{x}}_4(\widehat{z}(t)).\end{aligned} \tag{40}$$

Re-arrangement of (40) yields the following

$$\begin{aligned}\dot{e}(t) = & -e(t) + y(t) + \dot{y}(t) + \widehat{x}_2(t)\left(1 - \frac{1}{\widehat{R}_{ts}(\widehat{z}(t))\widehat{C}_{ts}(\widehat{z}(t))}\right) \\ & + \widehat{x}_3(t)\left(1 - \frac{1}{\widehat{R}_{tl}(\widehat{z}(t))\widehat{C}_{tl}(\widehat{z}(t))}\right) \\ & - \widehat{x}_1(\widehat{z}(t)) + i(t)\widehat{x}_4(\widehat{z}(t)) - \dot{\widehat{x}}_1(\widehat{z}(t)) \\ & + i(t)\left(\frac{1}{\widehat{C}_{ts}(\widehat{z}(t))} + \frac{1}{\widehat{C}_{tl}(\widehat{z}(t))}\right) + \frac{di(t)}{dt}\widehat{x}_4(\widehat{z}(t)) \\ & + i(t)\dot{\widehat{x}}_4(\widehat{z}(t)) + 2u(t).\end{aligned} \tag{41}$$

By definition in (23) and (24), because $\widehat{r}_n(t_0) > 0$ for $n \in \{1, 2, \ldots, 21\}\backslash\{3, 21\}$, and $\widehat{z}(t) = z(t)$ which belongs to [0,1]; so $\widehat{R}_{ts}(\widehat{z}(t)) > 0$, $\widehat{R}_{tl}(\widehat{z}(t)) > 0$ for all $t > t_0$. Also by Lemma 1, we know that $\widehat{C}_{ts}(\widehat{z}(t)) > 0$ and $\widehat{C}_{tl}(\widehat{z}(t)) > 0$ for all $t > t_0$. Therefore, $\widehat{R}_{ts}(\widehat{z}(t))\widehat{C}_{ts}(\widehat{z}(t)) > 0$ and $\widehat{R}_{tl}(\widehat{z}(t))\widehat{C}_{tl}(\widehat{z}(t)) > 0$.

$$\text{which implies } 1 - \frac{1}{\widehat{R}_{ts}(\widehat{z}(t))\widehat{C}_{ts}(\widehat{z}(t))} < 1, \tag{42}$$

From (18), $\widehat{x}_2(t) \geq 0$, Thus,

$$\widehat{x}_2(t)\left(1 - \frac{1}{\widehat{R}_{ts}(\widehat{z}(t))\widehat{C}_{ts}(\widehat{z}(t))}\right) \leq \widehat{x}_2(t), \tag{43}$$

Similarly using $\widehat{x}_3(t) \geq 0$ from (19) provides

$$\widehat{x}_3(t)\left(1 - \frac{1}{\widehat{R}_{tl}(\widehat{z}(t))\widehat{C}_{tl}(\widehat{z}(t))}\right) \leq \widehat{x}_3(t), \tag{44}$$

From (43) and (44) we get

$$\begin{aligned}\widehat{x}_2(t) + \widehat{x}_3(t) \geq & \; x_2(t)\left(1 - \frac{1}{\widehat{R}_{ts}(\widehat{z}(t))\widehat{C}_{ts}(\widehat{z}(t))}\right) \\ & + \widehat{x}_3(t)\left(1 - \frac{1}{\widehat{R}_{tl}(\widehat{z}(t))\widehat{C}_{tl}(\widehat{z}(t))}\right).\end{aligned} \tag{45}$$

Using (45) in (41) and re-arrangement of terms provides the following

$$\begin{aligned}\dot{e}(t) \leq & -e(t) + y(t) + \dot{y}(t) - \widehat{x}_1(\widehat{z}(t)) + \widehat{x}_2(t) + \widehat{x}_3(t) \\ & + i(t)\widehat{x}_4(\widehat{z}(t)) - \dot{\widehat{x}}_1(\widehat{z}(t)) + \frac{di(t)}{dt}\widehat{x}_4(\widehat{z}(t)) \\ & + i(t)\dot{\widehat{x}}_4(\widehat{z}(t)) + i(t)\left(\frac{1}{\widehat{C}_{ts}(\widehat{z}(t))} + \frac{1}{\widehat{C}_{tl}(\widehat{z}(t))}\right) \\ & + 2u(t).\end{aligned} \tag{46}$$

Simplification of (46) using (21) and (28) gives

$$\begin{aligned}\dot{e}(t) \leq & -y(t) + \widehat{y}(t) + y(t) + \dot{y}(t) - \dot{\widehat{y}}(t) - \dot{\widehat{x}}_1(\widehat{z}(t)) \\ & + \frac{di(t)}{dt}\widehat{x}_4(\widehat{z}(t)) + i(t)\dot{\widehat{x}}_4(\widehat{z}(t)) \\ & + i(t)\left(\frac{1}{\widehat{C}_{ts}(\widehat{z}(t))} + \frac{1}{\widehat{C}_{tl}(\widehat{z}(t))}\right) + 2u(t), \text{ i.e.}\end{aligned} \tag{47}$$

$$\dot{e}(t) \leq \dot{y}(t) - \dot{\widehat{x}}_1(\widehat{z}(t)) + \frac{di(t)}{dt}\widehat{x}_4(\widehat{z}(t)) + i(t)\dot{\widehat{x}}_4(\widehat{z}(t))$$

$$+ i(t)\left(\frac{1}{\widehat{C}_{ts}(\widehat{z}(t))} + \frac{1}{\widehat{C}_{tl}(\widehat{z}(t))}\right) + 2u(t). \tag{48}$$

Using (17) and (20) in (48) gives

$$\begin{aligned}\dot{e}(t) \leq\ & \dot{y}(t) - \frac{\partial \widehat{x}_1(\widehat{z}(t))}{\partial \widehat{z}(t)}\dot{\widehat{z}}(t) + \frac{di(t)}{dt}\widehat{x}_4(\widehat{z}(t)) \\ & + i(t)\frac{\partial \widehat{x}_4(\widehat{z}(t))}{\partial \widehat{z}(t)}\dot{\widehat{z}}(t) + i(t)u(t) \\ & + i(t)\left(\frac{1}{\widehat{C}_{ts}(\widehat{z}(t))} + \frac{1}{\widehat{C}_{tl}(\widehat{z}(t))}\right) + 3u(t). \end{aligned} \tag{49}$$

Following this, the proof of error $e(t)$ convergence to zero is derived from the equation (49). For the proof some inequalities are required to be established, which are first shown. Consider the following inequality related to $|e(t)|$ and the first term of R.H.S. of (49),

$$\begin{aligned}(|e(t)| - \dot{y}(t))^2 \ &\geq 0, \\ \frac{1}{2}|e(t)|^2 + \frac{1}{2}\dot{y}^2(t) &\geq |e(t)|\dot{y}(t). \end{aligned} \tag{50}$$

The inequality related to $|e(t)|$ and the second term of R.H.S. of (49) is as follows,

$$\begin{aligned}\left(|e(t)| + \frac{\partial \widehat{x}_1(\widehat{z}(t))}{\partial \widehat{z}(t)}\dot{\widehat{z}}(t)\right)^2 &\geq 0, \\ \frac{1}{2}|e(t)|^2 + \frac{1}{2}\left(\frac{\partial \widehat{x}_1(\widehat{z}(t))}{\partial \widehat{z}(t)}\dot{\widehat{z}}(t)\right)^2 &\geq -|e(t)|\frac{\partial \widehat{x}_1(\widehat{z}(t))}{\partial \widehat{z}(t)}\dot{\widehat{z}}(t). \end{aligned} \tag{51}$$

The inequality related to $|e(t)|$ and the third term of R.H.S. of (49) is given as,

$$\begin{aligned}\left(|e(t)| - \frac{di(t)}{dt}\widehat{x}_4(\widehat{z}(t))\right)^2 &\geq 0, \\ \frac{1}{2}|e(t)|^2 + \frac{1}{2}\left(\frac{di(t)}{dt}\right)^2\widehat{x}_4^2(\widehat{z}(t)) &\geq |e(t)|\frac{di(t)}{dt}\widehat{x}_4(\widehat{z}(t)). \end{aligned} \tag{52}$$

The inequality related to $|e(t)|$ and the fourth term of R.H.S. of (49) is as follows,

$$\begin{aligned}\left(|e(t)| - i(t)\frac{\partial \widehat{x}_4(\widehat{z}(t))}{\partial \widehat{z}(t)}\dot{\widehat{z}}(t)\right)^2 &\geq 0, \\ \frac{1}{2}|e(t)|^2 + \frac{1}{2}i^2(t)\left(\frac{\partial \widehat{x}_4(\widehat{z}(t))}{\partial \widehat{z}(t)}\dot{\widehat{z}}(t)\right)^2 &\geq |e(t)|i(t)\frac{\partial \widehat{x}_4(\widehat{z}(t))}{\partial \widehat{z}(t)}\dot{\widehat{z}}(t). \end{aligned} \tag{53}$$

The inequality related to $|e(t)|$ and the sixth term of R.H.S. of (49) is given below,

$$\begin{aligned}\left(|e(t)| - i(t)\left(\frac{1}{\widehat{C}_{ts}(\widehat{z}(t))} + \frac{1}{\widehat{C}_{tl}(\widehat{z}(t))}\right)\right)^2 &\geq 0, \\ \frac{1}{2}|e(t)|^2 + \frac{1}{2}i^2(t)\left(\frac{1}{\widehat{C}_{ts}(\widehat{z}(t))} + \frac{1}{\widehat{C}_{tl}(\widehat{z}(t))}\right)^2 &\geq |e(t)|i(t) \\ \times \left(\frac{1}{\widehat{C}_{ts}(\widehat{z}(t))} + \frac{1}{\widehat{C}_{tl}(\widehat{z}(t))}\right). \end{aligned} \tag{54}$$

From (50), (51), (52), (53), and (54), we get (55)

$$\begin{aligned}&\frac{5}{2}|e(t)|^2 + \frac{1}{2}\dot{y}^2(t) + \frac{1}{2}\left(\frac{\partial \widehat{x}_1(\widehat{z}(t))}{\partial \widehat{z}(t)}\dot{\widehat{z}}(t)\right)^2 \\ &+ \frac{1}{2}\left(\frac{di(t)}{dt}\right)^2\widehat{x}_4^2(\widehat{z}(t)) + \frac{1}{2}i^2(t)\left(\frac{\partial \widehat{x}_4(\widehat{z}(t))}{\partial \widehat{z}(t)}\dot{\widehat{z}}(t)\right)^2 \\ &+ \frac{1}{2}i^2(t)\left(\frac{1}{\widehat{C}_{ts}(\widehat{z}(t))} + \frac{1}{\widehat{C}_{tl}(\widehat{z}(t))}\right)^2 \\ &\geq \Bigg(|e(t)|\dot{y}(t) - |e(t)|\frac{\partial \widehat{x}_1(\widehat{z}(t))}{\partial \widehat{z}(t)}\dot{\widehat{z}}(t) + |e(t)|\frac{di(t)}{dt}\widehat{x}_4(\widehat{z}(t)) \\ &+ |e(t)|i(t)\frac{\partial \widehat{x}_4(\widehat{z}(t))}{\partial \widehat{z}(t)}\dot{\widehat{z}}(t) \\ &+ |e(t)|i(t)\left(\frac{1}{\widehat{C}_{ts}(\widehat{z}(t))} + \frac{1}{\widehat{C}_{tl}(\widehat{z}(t))}\right)\Bigg). \end{aligned} \tag{55}$$

Multiplying (49) by $|e(t)|$ and using (31) gives

$$\begin{aligned}|e(t)|\dot{e}(t) \leq\ & |e(t)|\dot{y}(t) - |e(t)|\frac{\partial \widehat{x}_1(\widehat{z}(t))}{\partial \widehat{z}(t)}\dot{\widehat{z}}(t) \\ & + |e(t)|\frac{di(t)}{dt}\widehat{x}_4(\widehat{z}(t)) \\ & + |e(t)|i(t)\frac{\partial \widehat{x}_4(\widehat{z}(t))}{\partial \widehat{z}(t)}\dot{\widehat{z}}(t) + |e(t)|i(t) \\ & \times \left(\frac{1}{\widehat{C}_{ts}(\widehat{z}(t))} + \frac{1}{\widehat{C}_{tl}(\widehat{z}(t))}\right) \\ & - (3 + i(t))N(k(t))|e(t)|e(t), \end{aligned} \tag{56}$$

Now use (55) in (56) to get the following

$$\begin{aligned}|e(t)|\dot{e}(t) \leq\ & \frac{5}{2}|e(t)|^2 + \frac{1}{2}\dot{y}^2(t) + \frac{1}{2}\left(\frac{\partial \widehat{x}_1(\widehat{z}(t))}{\partial \widehat{z}(t)}\dot{\widehat{z}}(t)\right)^2 \\ & + \frac{1}{2}\left(\frac{di(t)}{dt}\right)^2\widehat{x}_4^2(\widehat{z}(t)) + \frac{1}{2}i^2(t)\left(\frac{\partial \widehat{x}_4(\widehat{z}(t))}{\partial \widehat{z}(t)}\dot{\widehat{z}}(t)\right)^2 \\ & + \frac{1}{2}i^2(t)\left(\frac{1}{\widehat{C}_{ts}(\widehat{z}(t))} + \frac{1}{\widehat{C}_{tl}(\widehat{z}(t))}\right)^2 \\ & - (3 + i(t))N(k(t))|e(t)|e(t). \end{aligned} \tag{57}$$

Because $\frac{d}{dt}(\frac{1}{2}|e(t)|^2) = |e(t)|\frac{d}{dt}|e(t)| = |e(t)|\frac{d}{dt}(\sqrt{e^2(t)}) = |e(t)|\dot{e}(t)$, thus integrating (57) from t_0 to t, using the definition $|x| = \sqrt{x^2}$, and using (29) provides

$$\begin{aligned}\frac{1}{2}e^2(t) \leq\ & \frac{5}{2}(k(t) - k(t_0)) + \frac{1}{2}\int_{t_0}^{t}\dot{y}^2(\tau)d\tau \\ & + \frac{1}{2}\int_{t_0}^{t}\left(\frac{\partial \widehat{x}_1(\widehat{z}(\tau))}{\partial \widehat{z}(\tau)}\dot{\widehat{z}}(\tau)\right)^2 d\tau \\ & + \frac{1}{2}\int_{t_0}^{t}\left(\frac{di(\tau)}{d\tau}\right)^2\widehat{x}_4^2(\widehat{z}(\tau))d\tau \end{aligned}$$

$$+\frac{1}{2}\int_{t_0}^{t} i^2(\tau)\left(\frac{\partial \widehat{x}_4(\widehat{z}(\tau))}{\partial \widehat{z}(\tau)}\dot{\widehat{z}}(\tau)\right)^2 d\tau + \frac{1}{2}\int_{t_0}^{t} i^2(\tau)\left(\frac{1}{\widehat{C}_{ts}(\widehat{z}(\tau))}+\frac{1}{\widehat{C}_{tl}(\widehat{z}(\tau))}\right)^2 d\tau - 3\int_{t_0}^{t} N(k(\tau))\dot{k}(\tau)d\tau - \int_{t_0}^{t} i(\tau)N(k(\tau))\dot{k}(\tau)d\tau. \tag{58}$$

Let $\widetilde{k}(t) = k(t) - k(t_0)$. Dividing (58) by $\widetilde{k}(t)$ and recognizing that $\dot{\widehat{z}}(t) = -\frac{i(t)}{C_c}$, $\int_{t_0}^{t} N(k(\tau))\dot{k}(\tau)d\tau = \int_{k(t_0)}^{k(t)} N(k)dk$ and $\int_{t_0}^{t} i(\tau)N(k(\tau))\dot{k}(\tau)d\tau = i(t)\int_{k(t_0)}^{k(t)} N(k)dk$ gives

$$\frac{e^2(t)}{2\widetilde{k}(t)} \le \frac{5}{2} + \frac{1}{2\widetilde{k}(t)}\int_{t_0}^{t}\dot{y}^2(\tau)d\tau + \frac{1}{2\widetilde{k}(t)}\int_{t_0}^{t}\left(\frac{i(\tau)}{C_c}\frac{\partial \widehat{x}_1(\widehat{z}(\tau))}{\partial \widehat{z}(\tau)}\right)^2 d\tau + \frac{1}{2\widetilde{k}(t)}\int_{t_0}^{t}\left(\frac{di(\tau)}{d\tau}\right)^2 \widehat{x}_4^2(\widehat{z}(\tau))d\tau + \frac{1}{2\widetilde{k}(t)}\int_{t_0}^{t}\left(\frac{i^2(\tau)}{C_c}\frac{\partial \widehat{x}_4(\widehat{z}(\tau))}{\partial \widehat{z}(\tau)}\right)^2 d\tau + \frac{1}{2\widetilde{k}(t)}\int_{t_0}^{t} i^2(\tau)\left(\frac{1}{\widehat{C}_{ts}(\widehat{z}(\tau))}+\frac{1}{\widehat{C}_{tl}(\widehat{z}(\tau))}\right)^2 d\tau - \frac{3}{\widetilde{k}(t)}\int_{k(t_0)}^{k(t)} N(k)dk - \frac{i(t)}{\widetilde{k}(t)}\int_{k(t_0)}^{k(t)} N(k)dk. \tag{59}$$

Any battery can only be discharged for a certain interval of time, say $T' > t_0$. After time $t > T'$, the following occurs: $i(t) = 0$, $y(t) = 0$, $z(t) = 0$, because all the charge in the battery is exhausted. Therefore, as $t \to \infty$, $\dot{y}(t) = 0$, and $\frac{d(i)}{dt} = 0$. Thus, from these facts, we can conclude that the terms $\int_{t_0}^{t}\dot{y}^2(\tau)d\tau$, $\int_{t_0}^{t}\left(\frac{i(\tau)}{C_c}\frac{\partial \widehat{x}_1(\widehat{z}(\tau))}{\partial \widehat{z}(\tau)}\right)^2 d\tau$, $\int_{t_0}^{t}\left(\frac{di(\tau)}{d\tau}\right)^2 \widehat{x}_4^2(\widehat{z}(\tau))d\tau$, $\int_{t_0}^{t}\left(\frac{i^2(\tau)}{C_c}\frac{\partial \widehat{x}_4(\widehat{z}(\tau))}{\partial \widehat{z}(\tau)}\right)^2 d\tau$, and $\frac{1}{2}\int_{t_0}^{t} i^2(\tau)\left(\frac{1}{\widehat{C}_{ts}(\widehat{z}(\tau))}-\frac{1}{\widehat{C}_{tl}(\widehat{z}(\tau))}\right)^2 d\tau$ are bounded in (59) as $t \to \infty$. Now suppose that $k(t) \to \infty$ as $t \to \infty$, then the above discussion lets us write as $t \to \infty$ for (59),

$$\lim_{t\to\infty}\frac{e^2(t)}{2\widetilde{k}(t)} \le \frac{5}{2} - \frac{3}{\widetilde{k}(t)}\int_{k(t_0)}^{k(t)} N(k)dk - \frac{i(t)}{\widetilde{k}(t)}\int_{k(t_0)}^{k(t)} N(k)dk, \tag{60}$$

Now if $k(t) \to \infty$ as $t \to \infty$ then by the definition of a Nussbaum function in (13), the term $+\frac{1}{k(t)-k(t_0)}\int_{k(t_0)}^{k(t)} N(k)dk$, in (60) can take values approaching $+\infty$, and therefore this will violate the positiveness of the LHS of (60). By this contradiction, the assumption that $k(t) \to \infty$ is false, therefore $k(t)$ is bounded. However $\dot{k}(t)$ is an increasing function by definition and $k(t)$ is bounded, this implies that $k(t) \to k_\infty$ as $t \to \infty$ which further implies that $\dot{k}(t) \to 0$ as $t \to \infty$, i.e. $e^2(t) \to 0$ as $t \to \infty$ or $e(t) \to 0$ as $t \to \infty$, i.e. $y(t) \to \widehat{y}(t)$ as $t \to \infty$. The required result is achieved, thus completing the proof. □

The following results shows that the estimated values of Li-ion battery model parameters $\widehat{r}_n(t)$ converge.

Lemma 2: Suppose $\lambda_{xn}, \lambda_{yn}, r_{n_u}$ and r_{n_l} are positive real numbers for $n \in \{1, 2, \ldots, 21\}\backslash\{3, 21\}$. **If** the conditions required for Theorem 1 to hold are satisfied, **then** $\widehat{r}_n(t)$ converges to some constant r_∞ as $t \to \infty$.

Proof: The solution of (32) with $e^2(t) + \lambda_{x_n} r_{n_u} + \lambda_{y_n} r_{n_l}$ as an input is as follows

$$\widehat{r}_n(t) = \widehat{r}_n(t_0)e^{-(\lambda_{x_n}+\lambda_{y_n})t} + \left((\lambda_{x_n} r_{n_u} + \lambda_{y_n} r_{n_l}) \times \int_{t_0}^{t} e^{-(\lambda_{x_n}+\lambda_{y_n})\tau} d\tau\right) + \int_{t_0}^{t} e^2(t-\tau)e^{-(\lambda_{x_n}+\lambda_{y_n})\tau} d\tau \tag{61}$$

Because $e^{-(\lambda_{x_n}+\lambda_{y_n})t} \to 0$ as $t \to \infty$, and from Theorem 1, $e(t) \to 0$ as $t \to \infty$. So $e^{-(\lambda_{x_n}+\lambda_{y_n})t}$ and $e^2(t)$ remain positive and approach to zero as $t \to \infty$. Thus, on the R.H.S. of (61), the first term will go to zero, the second and third terms will be bounded and approach to a constant term as $t \to \infty$. Hence, $\widehat{r}_n(t)$ converges as $t \to \infty$ for $n \in \{1, 2, \ldots, 21\}\backslash\{3, 21\}$. □

Now that the above result has shown that the estimated parameters $\widehat{r}_n(t)$ for $n \in \{1, 2, \ldots, 21\}\backslash\{3, 21\}$, converge as $t \to \infty$; the following result shows that the estimated parameters $\widehat{r}_n(t)$ converge to their actual values r_n. Note that r_n are constants. Define the following variables.

$$\Delta x_j(t) = \widehat{x}_j(t) - x_j(t), \text{ for } j \in \{1, 2, 3, 4\} \tag{62}$$

$$\Delta r_n(t) = \widehat{r}_n(t) - r_n, \text{ for } n \in \{1, 2, \ldots, 21\}\backslash\{3, 21\} \tag{63}$$

$$\delta_1 = -\frac{1}{r_{14}}\ln\left(\frac{r_{15}}{r_{13}}\right) \tag{64}$$

$$\delta_2 = -\frac{1}{r_{17}}\ln\left(\frac{r_{18}}{r_{16}}\right) \tag{65}$$

$$\delta_3(t) = C_c\left(\frac{x_2(t)}{C_{ts}(z(t))} + \frac{x_3(t)}{C_{tl}(z(t))} + \frac{\widehat{x}_2}{\widehat{C}_{ts}(z(t))} + \frac{\widehat{x}_3}{\widehat{C}_{tl}(z(t))}\right). \tag{66}$$

Note also that the conditions $r_{13} > r_{15} > 0$, and $r_{16} > r_{18} > 0$ required in the result below are not artificial, but are a common and natural consequence of the shape of the terminal voltage curve, and a battery's electrical response time constants. In fact based on the work in [1] (which provides rigorous experimental verification), the authors in [24] have shown that battery model parameter values maintain such an order relation.

Theorem 2: Suppose the conditions required for Theorem 1 to hold are satisfied. Let ϵ be a positive real number, and let $t^*, T, z(t) \in \mathbb{R}$ such that $t^* < T$, and $z(t) \in [0, 1]$. Let $r_{13} > r_{15} > 0$, and $r_{16} > r_{18} > 0$. Suppose $M > i(t) > 0$, $i(t) \to 0$ as $t \to T$, and let $\frac{di(t)}{dt}$ be bounded for all $t \ge t_0$.

Given any ϵ, **if** $z(t) > \max\{\delta_1, \delta_2, \delta_3(t)\}$, and there exists a time instant t^* such that for all $t > t^*$ we have $|y(t) - \widehat{y}(t)| < \epsilon$, **then** $\Delta x_j(t), \Delta r_n(t) \to 0$ as $t \to \infty$. Here $j \in \{1, 2, 3, 4\}$, $n \in \{1, 2, \ldots, 21\}\backslash\{3, 21\}$.

Proof: To prove the intended result we start by examining the stability of the battery model states in (1)–(6) and the observer states in (16)–(19). Consider the candidate Lyapunov function as shown in (67).

$$V(z, x_2, x_3, \widehat{x}_2, \widehat{x}_3) = \frac{1}{2}z^2 + \frac{1}{2}\Sigma_{j=2}^{j=3}\left(x_j^2 + \widehat{x}_j^2\right) \tag{67}$$

$V(z, x_2, x_3, \widehat{x}_2, \widehat{x}_3) > 0$ for all $z, x_2, x_3, \widehat{x}_2, \widehat{x}_3 \neq 0$. Taking the time derivative of V provides the following, where the arguments of V are not written for brevity.

$$\dot{V} = z\dot{z} + \Sigma_{j=2}^{j=3}\left(x_j\dot{x}_j + \widehat{x}_j\dot{\widehat{x}}_j\right) \tag{68}$$

Now, as per the assumptions, we know that the conditions required for Theorem 1 to hold are satisfied. Therefore from Theorem 1 we know that $e(t) \to 0$ as $t \to \infty$. Which, by the definition of $e(t)$ in (28) and from basic definitions related to convergence [28], implies that there exists a time instant t^* such that for all $t > t^*$ we have $|y(t) - \widehat{y}(t)| < \epsilon$, for arbitrarily small positive ϵ. So, for $t > t^*$ and considering the fact that $e(t) \to 0$ as $t \to \infty$ gives us $u(t) \to 0$ as $t \to \infty$ based on (29)–(31). Subsequently, using equations (1), (3), (4), (18), and (19) with (68) considering $t > t^*$ results in,

$$\begin{aligned}\dot{V} = & -z(t)\frac{i(t)}{C_c} - \frac{x_2^2(t)}{R_{ts}(z)C_{ts}(z)} + \frac{i(t)x_2(t)}{C_{ts}(z)} \\ & - \frac{x_3^2(t)}{R_{tl}(z)C_{tl}(z)} + \frac{i(t)x_3(t)}{C_{tl}(z)} - \frac{\widehat{x}_2^2(t)}{\widehat{R}_{ts}(\widehat{z})\widehat{C}_{ts}(\widehat{z})} \\ & + \frac{i(t)\widehat{x}_2}{\widehat{C}_{ts}(\widehat{z})} - \frac{\widehat{x}_3^2(t)}{\widehat{R}_{tl}(\widehat{z})\widehat{C}_{tl}(\widehat{z})} + \frac{i(t)\widehat{x}_3}{\widehat{C}_{tl}(\widehat{z})}\end{aligned} \tag{69}$$

Re-arranging (69) gives

$$\begin{aligned}\dot{V} = & -\frac{x_2^2(t)}{R_{ts}(z)C_{ts}(z)} - \frac{x_3^2(t)}{R_{tl}(z)C_{tl}(z)} - \frac{\widehat{x}_2^2(t)}{\widehat{R}_{ts}(\widehat{z})\widehat{C}_{ts}(\widehat{z})} \\ & - \frac{\widehat{x}_3^2(t)}{\widehat{R}_{tl}(\widehat{z})\widehat{C}_{tl}(\widehat{z})} + i(t)\left(-\frac{z(t)}{C_c} + \frac{x_2(t)}{C_{ts}(z)}\right. \\ & \left. + \frac{x_3(t)}{C_{tl}(z)} + \frac{\widehat{x}_2}{\widehat{C}_{ts}(\widehat{z})} + \frac{\widehat{x}_3}{\widehat{C}_{tl}(\widehat{z})}\right)\end{aligned} \tag{70}$$

Now notice that as mentioned below (12) the actual parameters values $r_1, r_2 \ldots, r_{21}$ are all positive numbers. Thus from equations (8), (9), and knowing that the battery SoC $z(t) \in [0, 1]$ we know that $R_{ts}(z(t)), R_{tl}(z(t)) > 0$ for all time. Also By definition in (23) and (24), because $\widehat{r}_n(t_0) > 0$ for $n \in \{1, 2, \ldots, 21\}\backslash\{3, 21\}$, and $\widehat{z}(t) = z(t)$ by definition, and $z(t) \in [0, 1]$; so $\widehat{R}_{ts}(\widehat{z}(t)) > 0$, $\widehat{R}_{tl}(\widehat{z}(t)) > 0$ for all $t > t_0$. Further, the assumptions of this theorem require Theorem 1 to hold, which in turn requires the assumptions of Lemma 1 to be satisfied. Therefore, by Lemma 1 we have $\widehat{C}_{ts}(\widehat{z}(t)) > 0$, $\widehat{C}_{tl}(\widehat{z}(t)) > 0$ for all $t > t_0$. Now from the forms of $C_{ts}(z), C_{tl}(z)$ as seen in (10), (11), and by the assumptions of this theorem i.e. $r_{13} > r_{15} > 0$ and $r_{16} > r_{18} > 0$, so we can see that

$$C_{ts}(z) > 0, \text{ for } z > -\frac{1}{r_{14}}\ln\left(\frac{r_{15}}{r_{13}}\right), \tag{71}$$

$$C_{tl}(z) > 0, \text{ for } z > -\frac{1}{r_{17}}\ln\left(\frac{r_{18}}{r_{16}}\right). \tag{72}$$

Thus we can now say

$$\dot{V} < 0, \text{ for } z(t) > \max\{\delta_1, \delta_2, \delta_3(t)\}, \text{ where} \tag{73}$$

$$\delta_1 = -\frac{1}{r_{14}}\ln\left(\frac{r_{15}}{r_{13}}\right) \tag{74}$$

$$\delta_2 = -\frac{1}{r_{17}}\ln\left(\frac{r_{18}}{r_{16}}\right) \tag{75}$$

$$\delta_3(t) = C_c\left(\frac{x_2(t)}{C_{ts}(z(t))} + \frac{x_3(t)}{C_{tl}(z(t))} + \frac{\widehat{x}_2}{\widehat{C}_{ts}(z(t))} + \frac{\widehat{x}_3}{\widehat{C}_{tl}(z(t))}\right) \tag{76}$$

Therefore from results in Lyapunov stability analysis, we have that the dynamics of $x_2, x_3, \widehat{x}_2, \widehat{x}_3$ in (3), (4), (18), (19) are asymptotically stable, and $x_2(t), x_3(t), \widehat{x}_2(t), \widehat{x}_3(t) \to 0$, as $t \to \infty, t > t^*$, if $z(t) > \max\{\delta_1, \delta_2, \delta_3(t)\}$. Now let

$$X = [\Delta x_2 \quad \Delta x_3]^T \tag{77}$$

$$\varphi(X) = \frac{1}{2}X^TX \tag{78}$$

From the above discussion we know that all $x_j, \widehat{x}_j$, $j \in \{2, 3\}$ are bounded for $t \to \infty, t > t^*$, if $z(t) > \max\{\delta_1, \delta_2, \delta_3(t)\}$. This implies from the definition of Δx_j, Δr_n in (62), (63) that Δx_j are bounded for all j as $t \to \infty$. This implies that there exists a constant $c_1 < \infty$ such that

$$\lim_{t\to\infty}\varphi(X) \to c_1, \text{ if } z(t) > \max\{\delta_1, \delta_2, \delta_3(t)\}. \tag{79}$$

Now consider the first and second time derivatives of $\varphi(X)$.

$$\dot{\varphi}(X) = X^T\dot{X} \tag{80}$$

$$\ddot{\varphi}(X) = \dot{X}^T\dot{X} + X^T\ddot{X}, \text{ and} \tag{81}$$

$$\dot{X} = [\dot{\Delta}x_2 \quad \dot{\Delta}x_3]^T \tag{82}$$

$$\ddot{X} = [\ddot{\Delta}x_2 \quad \ddot{\Delta}x_3]^T. \tag{83}$$

Now as mentioned earlier in this proof, we know that $R_{ts}, R_{tl}, \widehat{R}_{ts}, \widehat{R}_{tl} > 0$ and by Lemma 1 we have $\widehat{C}_{ts}, \widehat{C}_{tl} > 0$ for all $t > t_0$. Further from (72), (73) we have that $C_{ts}, C_{tl} > 0$ for $z(t) > \max\{\delta_1, \delta_2\}$. Also we know that $e(t), u(t) \to 0$ as $t \to \infty, t > t^*$ and $M > i(t) > 0$ for all $t > t_0$. So, using the facts in this paragraph and considering the fact that $i(t)$ is bounded by assumption, and recalling that $x_2, x_3, \widehat{x}_2, \widehat{x}_3$ are bounded due to the asymptotic stability results derived above. Then from equations (2)–(5) and (17)–(20), it is trivial to see that $\dot{x}_j, \dot{\widehat{x}}_j$ and so by definition $\dot{\Delta}x_j$ are bounded for $t \in [t_0, \infty)$ for all $j \in \{2, 3\}$, if $z(t) > \max\{\delta_1, \delta_2, \delta_3(t)\}$. No consider $\ddot{x}_2, \ddot{x}_3$

as given below.

$$\ddot{x}_2 = -\frac{\dot{x}_2}{R_{ts}C_{ts}} - x_2\frac{d}{dt}\left(\frac{1}{R_{ts}C_{ts}}\right) + \frac{1}{C_{ts}}\frac{di(t)}{dt} + i(t)\frac{d}{dt}\frac{1}{C_{ts}} \tag{84}$$

$$\ddot{x}_3 = -\frac{\dot{x}_3}{R_{tl}C_{tl}} - x_3\frac{d}{dt}\left(\frac{1}{R_{tl}C_{tl}}\right) + \frac{1}{C_{tl}}\frac{di(t)}{dt} + i(t)\frac{d}{dt}\frac{1}{C_{tl}} \tag{85}$$

Now further because $e(t), u(t) \to 0$ as $t \to \infty$, so consider $\ddot{\hat{x}}_2, \ddot{\hat{x}}_3$ as below.

$$\ddot{\hat{x}}_2 = -\frac{\dot{\hat{x}}_2}{\widehat{R}_{ts}\widehat{C}_{ts}} - \hat{x}_2\frac{d}{dt}\left(\frac{1}{\widehat{R}_{ts}\widehat{C}_{ts}}\right) + \frac{1}{\widehat{C}_{ts}}\frac{di(t)}{dt} + i(t)\frac{d}{dt}\frac{1}{\widehat{C}_{ts}} \tag{86}$$

$$\ddot{\hat{x}}_3 = -\frac{\dot{\hat{x}}_3}{\widehat{R}_{tl}\widehat{C}_{tl}} - \hat{x}_3\frac{d}{dt}\left(\frac{1}{\widehat{R}_{tl}\widehat{C}_{tl}}\right) + \frac{1}{\widehat{C}_{tl}}\frac{di(t)}{dt} + i(t)\frac{d}{dt}\frac{1}{\widehat{C}_{tl}} \tag{87}$$

Also, notice that

$$\frac{d}{dt}\frac{1}{R_{ts}} = \frac{-r_7r_8e^{-r_8z}}{R_{ts}^2}\left(\frac{-i(t)}{C_c}\right) \tag{88}$$

$$\frac{d}{dt}\frac{1}{R_{tl}} = \frac{-r_{10}r_{11}e^{-r_{11}z}}{R_{tl}^2}\left(\frac{-i(t)}{C_c}\right) \tag{89}$$

$$\frac{d}{dt}\frac{1}{C_{ts}} = \frac{r_{13}r_{14}e^{-r_{14}z}}{C_{ts}^2}\left(\frac{-i(t)}{C_c}\right) \tag{90}$$

$$\frac{d}{dt}\frac{1}{C_{tl}} = \frac{r_{16}r_{17}e^{-r_{17}z}}{C_{tl}^2}\left(\frac{-i(t)}{C_c}\right) \tag{91}$$

and,

$$\frac{d}{dt}\left(\frac{1}{R_{ts}C_{ts}}\right) = \frac{d}{dt}\left(\frac{1}{R_{ts}}\right)\frac{1}{C_{ts}} + \frac{1}{R_{ts}}\frac{d}{dt}\left(\frac{1}{C_{ts}}\right) \tag{92}$$

$$\frac{d}{dt}\left(\frac{1}{R_{tl}C_{tl}}\right) = \frac{d}{dt}\left(\frac{1}{R_{tl}}\right)\frac{1}{C_{tl}} + \frac{1}{R_{tl}}\frac{d}{dt}\left(\frac{1}{C_{tl}}\right) \tag{93}$$

similarly we get

$$\frac{d}{dt}\frac{1}{\widehat{R}_{ts}} = \frac{-\widehat{r}_7\widehat{r}_8e^{-\widehat{r}_8z}}{\widehat{R}_{ts}^2}\left(\frac{-i(t)}{C_c}\right) \tag{94}$$

$$\frac{d}{dt}\frac{1}{\widehat{R}_{tl}} = \frac{-\widehat{r}_{10}\widehat{r}_{11}e^{-\widehat{r}_{11}z}}{\widehat{R}_{tl}^2}\left(\frac{-i(t)}{C_c}\right) \tag{95}$$

$$\frac{d}{dt}\frac{1}{\widehat{C}_{ts}} = \frac{\widehat{r}_{13}\widehat{r}_{14}e^{-\widehat{r}_{14}z}}{\widehat{C}_{ts}^2}\left(\frac{-i(t)}{C_c}\right) \tag{96}$$

$$\frac{d}{dt}\frac{1}{\widehat{C}_{tl}} = \frac{\widehat{r}_{16}\widehat{r}_{17}e^{-\widehat{r}_{17}z}}{\widehat{C}_{tl}^2}\left(\frac{-i(t)}{C_c}\right) \tag{97}$$

and

$$\frac{d}{dt}\left(\frac{1}{\widehat{R}_{ts}\widehat{C}_{ts}}\right) = \frac{d}{dt}\left(\frac{1}{\widehat{R}_{ts}}\right)\frac{1}{\widehat{C}_{ts}} + \frac{1}{\widehat{R}_{ts}}\frac{d}{dt}\left(\frac{1}{\widehat{C}_{ts}}\right) \tag{98}$$

$$\frac{d}{dt}\left(\frac{1}{\widehat{R}_{tl}\widehat{C}_{tl}}\right) = \frac{d}{dt}\left(\frac{1}{\widehat{R}_{tl}}\right)\frac{1}{\widehat{C}_{tl}} + \frac{1}{\widehat{R}_{tl}}\frac{d}{dt}\left(\frac{1}{\widehat{C}_{tl}}\right). \tag{99}$$

Now as mentioned earlier in this proof, we know that $R_{ts}, R_{tl}, \widehat{R}_{ts}, \widehat{R}_{tl} > 0$ and by Lemma 1 we have $\widehat{C}_{ts}, \widehat{C}_{tl} > 0$ for all $t > t_0$. Further from (71), (72) we have that $C_{ts}, C_{tl} > 0$ for $z(t) > \max\{\delta_1, \delta_2\}$. Also $z \in [0, 1]$ and we are given that $\frac{di(t)}{dt}$ is bounded for all time. So, from (84)–(99), and because $\dot{x}_j, \dot{\hat{x}}_j$ are bounded as discussed earlier, we see that $\ddot{x}_j, \ddot{\hat{x}}_j$ and so by definition $\ddot{\Delta}x_j$ are bounded for $t \in [t_0, \infty)$ for all $j \in \{2, 3\}$, if $z(t) > \max\{\delta_1, \delta_2, \delta_3(t)\}$. Which also gives from (80) to (83) that $\ddot{\varphi}(X)$ is uniformly bounded and therefore $\dot{\varphi}(X)$ is uniformly continuous. Now recalling from earlier that $0 \leq \lim_{t\to\infty}\varphi(X) \leq c_1 < \infty$ and therefore invoking Barbalat's Lemma [29] we have that $\dot{\varphi}(X) \to 0$ as $t \to \infty$. Which gives us

$$\Delta x_2\dot{\Delta}x_2 + \Delta x_3\dot{\Delta}x_3 \to 0 \text{ as } t \to \infty, \tag{100}$$

if $z(t) > \max\{\delta_1, \delta_2, \delta_3(t)\}$. Now because $i(t), u(t) \to 0$, as $t \to \infty$ and all the actual and estimated resistances and capacitances are non-zero and positive if $z(t) > \max\{\delta_1, \delta_2, \delta_3(t)\}$ we can write for $t \to \infty$

$$\Delta x_2\dot{\Delta}x_2 = (\widehat{x}_2 - x_2)\left(\frac{-\widehat{x}_2}{\widehat{R}_{ts}\widehat{C}_{ts}} + \frac{x_2}{R_{ts}C_{ts}}\right) \tag{101}$$

$$\Delta x_3\dot{\Delta}x_3 = (\widehat{x}_3 - x_3)\left(\frac{-\widehat{x}_3}{\widehat{R}_{tl}\widehat{C}_{tl}} + \frac{x_3}{R_{tl}C_{tl}}\right). \tag{102}$$

Add and subtract $\frac{x_2}{\widehat{R}_{ts}\widehat{C}_{ts}}$ and $\frac{x_3}{\widehat{R}_{tl}\widehat{C}_{tl}}$ into (101)–(102) respectively and re-arrange to get

$$\Delta x_2\dot{\Delta}x_2 = (\widehat{x}_2 - x_2)\left(\frac{x_2 - \widehat{x}_2}{\widehat{R}_{ts}\widehat{C}_{ts}} + x_2\left(\frac{1}{R_{ts}C_{ts}} - \frac{1}{\widehat{R}_{ts}\widehat{C}_{ts}}\right)\right) \tag{103}$$

$$\Delta x_3\dot{\Delta}x_3 = (\widehat{x}_3 - x_3)\left(\frac{x_3 - \widehat{x}_3}{\widehat{R}_{tl}\widehat{C}_{tl}} + x_3\left(\frac{1}{R_{tl}C_{tl}} - \frac{1}{\widehat{R}_{tl}\widehat{C}_{tl}}\right)\right). \tag{104}$$

Now as $z(t) > \max\{\delta_1, \delta_2, \delta_3(t)\}$ so $x_2, x_3 \to 0$ as $t \to \infty$ so the second term in the second parentheses in (103), (104) vanishes giving us

$$\Delta x_2\dot{\Delta}x_2 + x_3\dot{\Delta}x_3 = -\left(\frac{(\widehat{x}_2 - x_2)^2}{\widehat{R}_{ts}\widehat{C}_{ts}} + \frac{(\widehat{x}_3 - x_3)^2}{\widehat{R}_{tl}\widehat{C}_{tl}}\right) \tag{105}$$

So we see from (100) and (105) that $\hat{x}_j \to x_j$ for $j \in \{2, 3\}$ if $z(t) > \max\{\delta_1, \delta_2, \delta_3(t)\}$. Now using this with the fact that $e(t) \to 0$ we can write the following using definitions of e, y and $\hat{y}$. There exists a time $t > t^*$ such that

$$|x_1 - \widehat{x}_1 + i(\widehat{x}_4 - x_4)| < \epsilon. \tag{106}$$

Let $t > T$ then we see that $i(t) \to 0$ as $t \to \infty, t > T > t^*$ and from (106) we have $\widehat{x}_1 \to x_1$.

At this point we proceed by contradiction. Let us suppose that the estimated parameters $\hat{r}_n$ and $\widehat{x}_4$ do not converge to r_n, x_4 respectively. Here $n \in \{1, 2, \ldots, 21\}\backslash\{3, 21\}$. This means that the parameters $\widehat{r}_3, \widehat{r}_{21}$ which are calculated based on these as in (33), (34), also do not converge. So this implies from definitions that $\widehat{E}_0, \widehat{R}_{ts}, \widehat{R}_{tl}, \widehat{C}_{ts}, \widehat{C}_{tl}$ do not converge to $E_0, R_{ts}, R_{tl}, C_{ts}, C_{tl}$. Which further implies from equations

(1)–(4), (7), and (16)–(19), (23) that that $\widehat{x}_j$ do not converge to x_j for $j \in \{1, 2, 3\}$. This contradicts what we have from above, so by this contradiction we have that the parameters involved in the circuit elements (1)–(4), (7) and (16)–(19), (23) do converge. Now let us also assume that $\hat{x}_4$ does not converge to x_4. Consider the fact that Theorem 1 holds, and does not require $i(t) \to 0$ and gives $e(t) \to 0$ as $t \to \infty$. Considering this with the fact that we have shown $\widehat{x}_j \to x_j$ for $j \in \{1, 2, 3\}$ we can use definitions of e, y and $\hat{y}$, to get by Theorem 1 that there exists a time t^* such that for all $t > t^*$ we have $|i(\widehat{x}_4 - x_4)| < \epsilon$. This contradicts our assumption that $\hat{x}_4$ does not converge to x_4. Further let us assume that $\widehat{r}_{19}, \widehat{r}_{20}$ do not converge to r_{19}, r_{20} respectively and therefore neither does $\widehat{r}_{21}$ which is calculated based on (34). If this is true, then this means that $\widehat{R}_s$ does not converge to R_s. But by definition in (27) and (12) we know that $\widehat{R}_s \equiv \widehat{x}_4$, $R_s \equiv x_4$. And we know from above that $\widehat{x}_4$ converges to x_4. This means that having $\widehat{R}_s$ not converge to R_s causes a contradiction.

So by all of the above contradictions together we get the required result, i.e. $\Delta x_j(t), \Delta r_n(t) \to 0$ as $t \to \infty$ if $z(t) > \max\{\delta_1, \delta_2, \delta_3(t)\}$, or in other words the estimated states and the parameters values converge to their actual values as long as the battery SoC does not fall below a certain low level. Calculation of the other two parameters $\widehat{r}_3, \widehat{r}_{21}$ require the states and the other parameters values as per (33) and (34), which having converged, provide the correct estimates for $\widehat{r}_3, \widehat{r}_{21}$. As the parameters estimates converge to the ideal values, this implies that the estimated values of the circuit elements also converge to their actual values. □

V. VALIDATION AT THE CELL LEVEL

The proposed methodology for the convergence of estimated values to their actual values, is verified by MATLAB simulation results. The accuracy of estimated circuit elements and their parameters is validated in simulation, by comparing the estimated values with the ones provided by Chen and Mora [1] for a 4.1 V, 850 mAh Li-ion battery. For simulation we consider a 4.1 V, 270 mAh Li-ion battery cell. Note that the difference in mAh only changes the value of C_c but does not affect the values of any other parameters. A lower value of 270 mAh is chosen so that the simulation time for a complete discharge cycle is not too long. The results provide estimated values of parameters close to those in [1].

The results form Chen and Mora's (CM) work [1] are considered as actual values for the case of 4.1 V cell. This is because, the authors in [1] performed 40 experiments, ten discharging curves each at 80, 160, 320, and 640 mA, to extract equivalent circuit elements of a Li-ion battery. These parameters are able to predict Li-ion battery voltage at any load profile within a 30 mV maximum voltage estimation error. Therefore, owing to high accuracy of the CM work and its extensive utilization in many of the state-of-the-art research studies, we refer to equivalent circuit parameters from the CM work as actual values, and use these parameter values as actual values for comparison purposes in this section. The parameters adaptation process begins with the appropriate choice of some constraints. These constraints include the selection of steady-state upper and lower bounds and their respective confidence levels for each parameter, described in Table 1. The initial values for the observer states are also selected as follows: $\widehat{x}_1(0) = E_o(0), \widehat{x}_2(0) = 0, \widehat{x}_3(0) = 0, \widehat{x}_4(0) = 0$, and $\widehat{y}(0) = y(0)$. The proposed approach is run in MATLAB for real-time parameters estimation of a Li-ion battery using a constant discharge current of 0.1 A. The estimated values of the parameters are shown in Table 1. The results in Table 1 show that the estimation error is less than 5% for most of the estimated parameters. This level of accuracy is achieved despite the selection of initial values of parameter estimates being far off from their actual values. The estimated parameters are then employed to analyze the variation of circuit elements values with SoC. The variation of the estimated and actual circuit elements values $E_0, R_s, R_{ts}, R_{tl}, C_{ts}$ and C_{tl} versus SoC are shown in the left subplots of Fig. 3(a)–(f) respectively. The right subplots of Fig. 3(a)–(f) show the respective estimation errors. The Chen and Mora's results are used as *actual values* in these.

All the circuit elements converged within a 10% error bound, except R_{ts} which can be further improved by fixing the upper and lower bounds appropriately. It can be noticed that estimation error of circuit elements is higher when SoC approaches zero. A Li-ion battery becomes unstable when the SoC value becomes lower than a certain threshold [24], which causes the estimated parameters to diverge from their actual values. Therefore, in this work the battery model parameters are estimated until the SoC is reduced to 7%, though the results in Fig. 3 are displayed until the SoC reaches 1%.

Further, we construct and test two 4.1 V, 275 mAh Li-ion battery models in simulation for validating the estimated parameters results against those obtained by Chen and Mora [1]. The first model contains the parameters estimated by the proposed method, while the second one, set as a reference model, uses Chen and Mora's [1] parameters. Each battery model is subjected to a random discharge current as shown in Fig. 4, and their open circuit and terminal voltages are compared in Fig. 5(a) and (c), respectively. While their respective estimation errors are plotted in Fig. 5(b) and (d), respectively. The low estimation error in both the open circuit and terminal voltage profiles in Fig. 5(b) and (d) show the accuracy of the proposed strategy.

Finally, the estimated parameters are used to determine the SoC using the open circuit voltage via interpolation [2], with the discharge current shown in Fig. 4. The estimated SoC and the one obtained by conventional Coulomb counting method are plotted in Fig. 5(e), while their difference is presented in Fig. 5(f). Fig. 5(g) and (h) show zoomed views of Fig. 5(e) and (f) for the SoC estimation. Since the error in Fig. 5(e) and (f) is relatively high in the 20 to 30 minute interval, so this range is zoomed in and shown in Fig. 5(g) and (h). It is still worth noting that the maximum error is under 5×10^{-3}.

TABLE 1 Simulation Results of a 4.1 V, 270 mAh Li-Ion Battery Model Parameters Estimation Test at the Cell Level

Parameter	Upper bound (r_{nu})	Lower bound (r_{nl})	λ_{x_n}	λ_{y_n}	Initial value	Estimated value	Desired value [1]	Estimation error (%)
$\widehat{r}_1$	4	0.1	20	65	100	1.0176	1.031	1.3
$\widehat{r}_2$	50	25	50	70	2000	35.4167	35	1.2
$\widehat{r}_3$	–	–	–	–	–	3.6855	3.685	0.014
$\widehat{r}_4$	0.5	0.1	30	70	50	0.22	0.2156	2.04
$\widehat{r}_5$	0.5	0.01	20	70	30	0.1189	0.1178	0.934
$\widehat{r}_6$	0.5	0.1	60	50	200	0.3182	0.3201	0.594
$\widehat{r}_7$	1	0.1	50	50	180	0.3002	0.3208	6.42
$\widehat{r}_8$	50	10	50	50	1700	30	29.14	2.95
$\widehat{r}_9$	0.1	0.01	50	50	240	0.055	0.04669	17.79
$\widehat{r}_{10}$	10	1	70	50	3600	6.2533	6.603	5.3
$\widehat{r}_{11}$	200	100	50	50	9300	149.9	155.2	3.41
$\widehat{r}_{12}$	0.1	0.01	50	50	264	0.0553	0.04984	10.95
$\widehat{r}_{13}$	1000	500	60	55	50000	760.869	752.9	1.06
$\widehat{r}_{14}$	30	1	5	10	1000	10.6672	13.51	21.04
$\widehat{r}_{15}$	800	500	80	50	50000	684.62	703.6	2.69
$\widehat{r}_{16}$	7000	5000	10	10	50000	6000	6056	0.92
$\widehat{r}_{17}$	50	5	50	50	1000	27.5	27.12	1.40
$\widehat{r}_{18}$	5000	3000	50	50	50000	4500	4475	0.558
$\widehat{r}_{19}$	0.5	0.01	20	50	60	0.15	0.1562	3.97
$\widehat{r}_{20}$	50	15	30	80	1200	24.5455	24.37	0.72
$\widehat{r}_{21}$	–	–	–	–	–	0.0826	0.07446	10.93

VI. EXPERIMENTAL VALIDATION ON A 22.2 V, 6.6 AH LITHIUM-POLYMER BATTERY PACK

This section demonstrates rigorous experimental verification of the proposed online APE strategy on a 22.2 V, 6.6 Ah, 6 cell Li-ion battery, for sixteen different discharging and sixteen constant current charging profiles. The details of these charge and discharge profiles are in [2]. The batteries are discharged up to 7% of their rated capacity in about 15 hours. The measured battery discharging current, measured and estimated terminal voltage during the proposed online APE strategy, are plotted in Fig. 6 subplots (a) and (b) respectively.

The battery parameters, $\widehat{r}_1, \ldots, \widehat{r}_{21}$ are estimated online using the proposed algorithm and recorded in 21 separate arrays. The initial values, steady-state upper and lower bounds chosen for the estimated parameters should satisfy the conditions mentioned in Lemmas 1, 2. The battery terminal voltage is estimated and compared with the actual voltage. The value of the estimated parameters is picked and considered a good estimate, when the terminal voltage estimation error gets below the user defined error bound. The average value of such good estimates of a particular parameter is finally considered as the estimated parameter's value, and the estimation process is ended.

The sampling time of the discharging voltage and current is set to 0.01 seconds, and the final values of the estimated parameters are obtained in about two seconds when the battery terminal voltage estimation error decreased to 0.1×10^{-5}. The results of estimated parameters obtained from the proposed online APE strategy are provided in Table 2, and are compared with the results of the reference offline APE technique shared in [2]. In Table 2, we use the values from [2] as benchmark for 22.2 V, 6.6 Ah Lithium-ion battery. The authors in [2] perform 32 experiments, sixteen different discharging and sixteen constant charging profiles. The average error for a set of sixteen different discharging profiles is 0.1%, and 1.7% for sixteen constant charging profiles. Therefore, owing to high accuracy of parameters provided in [2], we use them as reference in Table 2. Note that in Table 2, values related to parameters $\widehat{r}_3$ and $\widehat{r}_{21}$ are shown by dashes. This is because $\widehat{r}_3$ and $\widehat{r}_{21}$ disappear from the observer equations used in the proposed online APE strategy. So, parameters $\widehat{r}_3$ and $\widehat{r}_{21}$ are not estimated adaptively, but are calculated using equations (33)–(34).

For testing performance during discharging, sixteen different discharging load profiles as mentioned in [2] are successively applied to 22.2 V, 6.6 Ah Li-ion battery packs and the battery terminal voltage is estimated online using the acquired battery model.

As a sample, the estimated and measured terminal voltages along with the absolute voltage estimation error for two of the sixteen discharging load profiles are shown in Figs. 7 and 8. The terminal voltage estimation error data, for all sixteen discharging profiles, is stacked together to form a single large 'error array' of 2.75e7 samples. The mean value of the error array for proposed and reference APE methods are 0.0211 V and 0.0218 V, respectively. Whereas, the median value of the error array for proposed and reference APE methods are 0.027 V and 0.0143 V, respectively. Similarly, the mode value for proposed and reference APE methods are −0.4038 V and −0.347 V, respectively. Likewise, the standard deviation value for proposed and reference APE methods are found to be

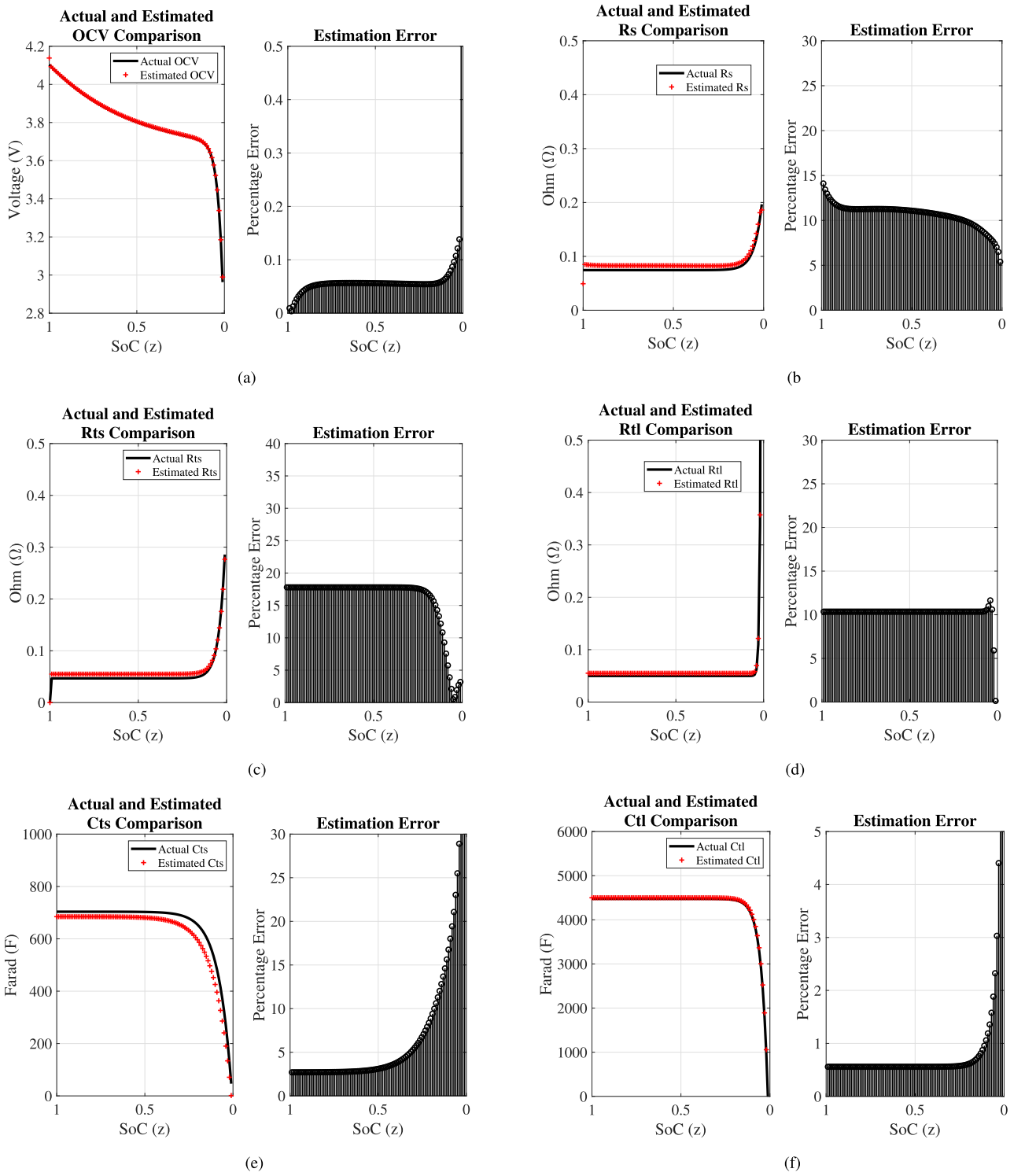

FIGURE 3. **Comparison of actual and estimated circuit elements of a 4.1 V, 270 mAh Li-ion battery model at the cell level. (a) Open circuit voltage E_o VS SoC. (b) Series resistance R_s VS SoC. (c) Short term resistance R_{ts} VS SoC. (d) Long term resistance R_{tl} VS SoC. (e) Short term capacitance C_{ts} VS SoC. (f) Long term capacitance C_{tl} VS SoC.**

0.5026 V and 0.5139 V, respectively. The Cumulative distribution graph of this terminal voltage estimation error array is shown in Fig. 10 respectively. Where, the red vertical lines in Fig. 10 indicate the ±4.5% terminal voltage estimation error limits, i.e. ± 1 V. Fig. 10 shows no significant difference between the proposed online APE results compared to the reference offline APE technique.

The estimated parameters obtained from the proposed online APE strategy are further assessed against the results obtained using the reference offline APE technique for

TABLE 2 Experimental Results of a 22 V, 6.6 Ah Li-Ion Battery Model Parameters Estimation Test at the Pack Level

Parameter	Upper bound (r_{nu})	Lower bound (r_{nl})	λ_{x_n}	λ_{y_n}	Initial value	Estimated value	Estimated value provided in [2]	Estimation error (%)
$\widehat{r}_1$	6	4	50	50	100	5	5.112	2.19
$\widehat{r}_2$	50	30	50	50	2000	40	40.955	2.33
$\widehat{r}_3$	–	–	–	–	–	22.1782	22.195	0.07
$\widehat{r}_4$	3	1	50	50	50	2	1.9215	4.08
$\widehat{r}_5$	2.5	1	50	50	30	1.75	1.759	0.51
$\widehat{r}_6$	4	2	50	50	200	3	3.0435	1.43
$\widehat{r}_7$	1	0.1	50	50	180	0.5505	0.5505	0
$\widehat{r}_8$	50	10	50	50	1700	30	30.0475	0.16
$\widehat{r}_9$	0.1	0.01	50	50	240	0.055	0.0551	0.18
$\widehat{r}_{10}$	10	1	70	50	3600	6.2557	6.2585	0.04
$\widehat{r}_{11}$	50	10	50	50	9300	30	30	0
$\widehat{r}_{12}$	0.1	0.01	50	50	264	0.0555	0.0551	0.73
$\widehat{r}_{13}$	1000	500	60	55	50000	760.8691	760.2266	0.08
$\widehat{r}_{14}$	15	5	70	50	1000	10.8334	10.7686	0.60
$\widehat{r}_{15}$	800	500	80	50	50000	684.615	685.7457	0.16
$\widehat{r}_{16}$	7000	5000	10	10	50000	6000	6036.4	0.60
$\widehat{r}_{17}$	50	5	50	50	1000	27.5	27.5422	0.15
$\widehat{r}_{18}$	5000	3000	10	20	50000	3667	3696	0.78
$\widehat{r}_{19}$	0.1	0.01	50	50	60	0.0551	0.0439	25.5
$\widehat{r}_{20}$	70	50	50	50	1200	60	59.07	1.57
$\widehat{r}_{21}$	–	–	–	–	–	0.2408	0.2246	7.21

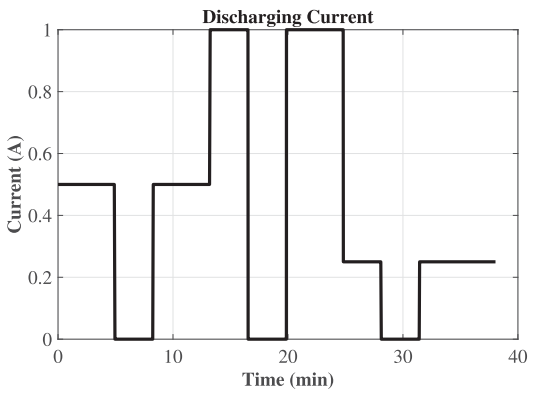

FIGURE 4. Variable current drawn from Li-ion battery.

sixteen constant current charging protocols. The actual Lipo battery is charged with a constant current of 2.5 amperes using the Thunder-Power charger (TP820CD). As a sample, the estimated and measured terminal voltages along with the absolute voltage estimation error for a single charging test, are shown in Fig. 9. The total number of samples collected in the terminal voltage estimation 'error array' while charging the batteries are 1.258e7, for both the proposed and reference APE methods. The cumulative distribution graph of the error array is shown Fig. 11, respectively, for both the proposed and reference APE strategies. The mean value of the error array for proposed and reference APE methods are -0.6518 V and -0.7080 V, respectively. Whereas, the median value of the error array for proposed and reference APE methods are -0.6451 V and -0.7059 V, respectively. Similarly, the mode value for proposed and reference APE methods are -2.1223 V and -2.1470 V, respectively. Likewise, the standard deviation value for proposed and reference APE methods are found to be 0.2271 V and 0.2231 V, respectively. This shows that the proposed online APE strategy produces results that are comparable to the reference offline APE technique while charging a Li-po battery.

To further test the accuracy of the parameters values estimated, the open circuit voltage and the series resistance variation vs. SoC is compared against measured values, for the 22.2 V, 6.6Ah battery pack. The results are shown in Figs. 12 and 13. The upper part of Fig. 12 shows the measured pack level OCV for a 22.2 V 6.6Ah Li-ion battery pack with 6 cells, and also shows the OCV estimated using the parameters estimated - as shown in Table 2. The lower part of Fig. 12 shows the error between the measured and estimated OCV. It is thus observed that the average error is around 0.8538 V, which is about a 3.85% error for a pack rated at 22.2 V. Similarly, Fig. 13 compares the battery series resistance vs. SoC curve estimated using the using the parameters estimated - as shown in Table 2, and values available in the literature [2] for the series resistance of the same battery pack used in this work. It is worth noting that the values from [2] are used for comparison as they have been verified by the authors in [2] through many experimental efforts, and also the OCV and series resistance parameters in [2] are not estimated using any filtering/estimation methodology, but by simply curve fitting using experimental data. From the lower part of Fig. 13 we can see that for SoC above 0.1 the error is lower than 0.02Ω or around 7% compared to the desired value. The error increases to about 10%, or 0.025Ω for values of SoC much lesser than 0.1. So from this, and from the terminal voltage estimation performance seen in Figs. 7–9 using the parameters estimated and shown in Table 2, we see that the proposed on-line adaptive parameters estimation method produces

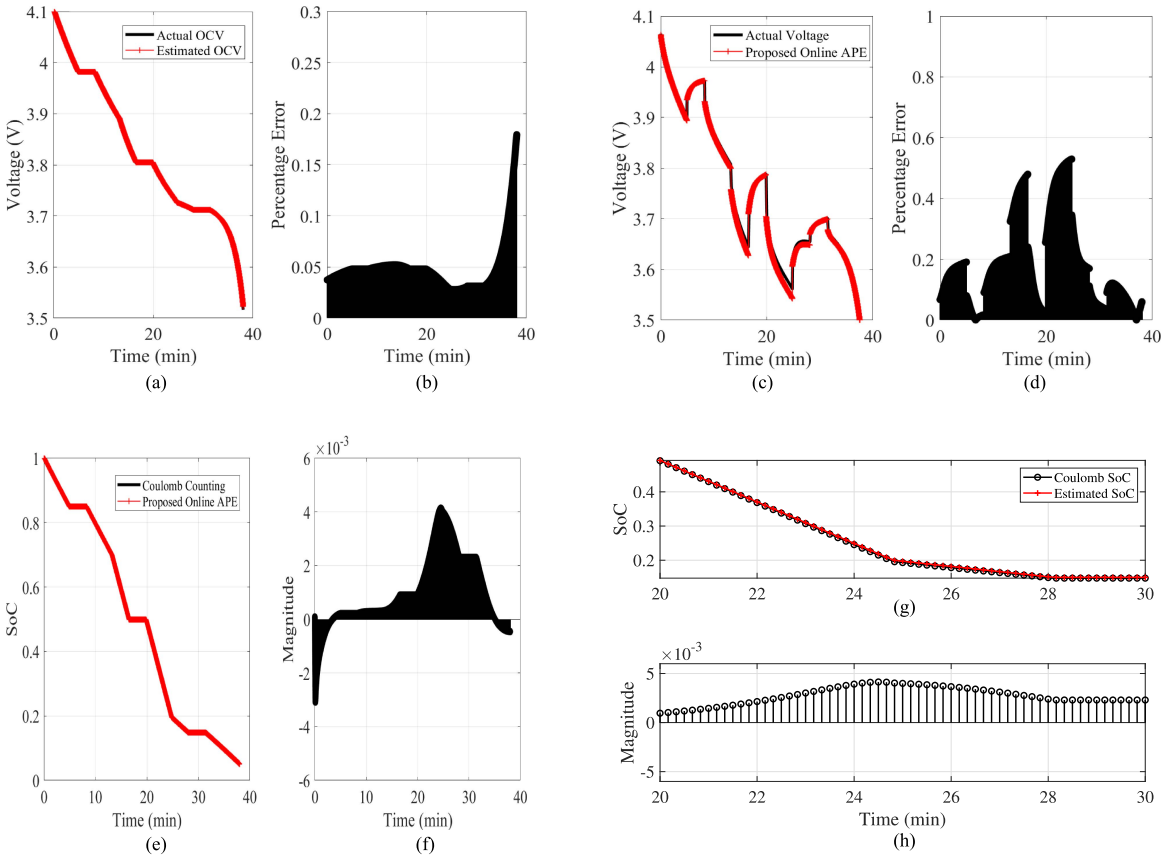

FIGURE 5. Validation of estimated OCV and terminal voltage of a Li-ion battery cell, and comparison of estimated SoC with Coulomb counting SoC when the battery is subjected to variable load. Sub-figures (g) and (h) show zoomed in view of portions of sub-figures (e) and (f) respectively. (a) Actual and estimated OCV. (b) Estimation error. (c) Actual and estimated terminal voltage. (d) Estimation error. (e) Coulomb counting and estimated SoC. (f) SoC estimation error with respect to coulomb counting. (g) Coulomb counting and estimated SoC. (h) SoC estimation error with respect to coulomb counting.

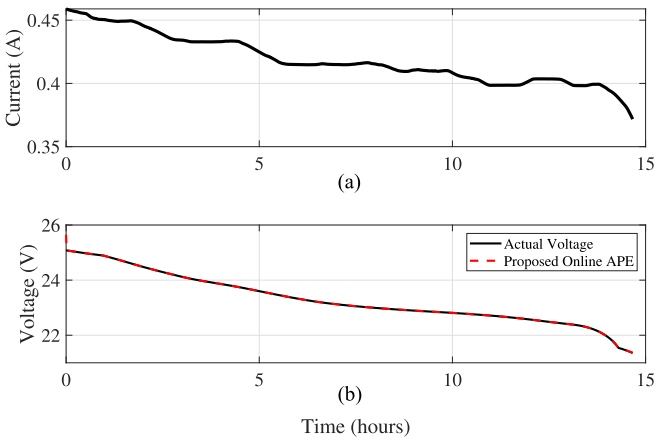

FIGURE 6. 22.2 V, 6.6Ah Lithium-Polymer battery pack discharging current and voltage profiles during adaptation process. (a) Discharging current. (b) Discharging voltage.

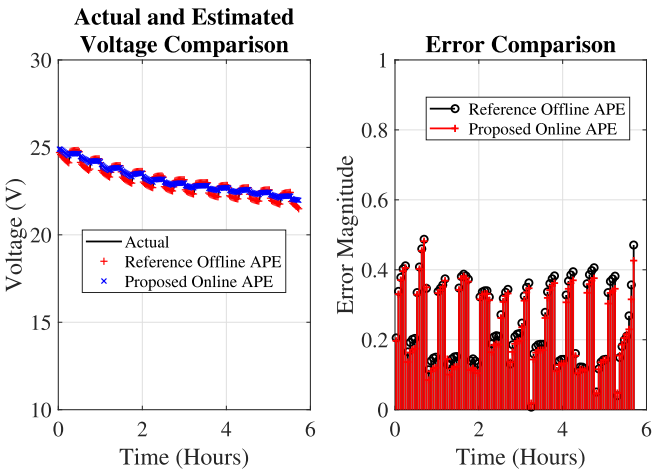

FIGURE 7. Terminal voltage estimation and absolute error $|e(t)|$ comparison for resistive load of 11.11 Ω with 15 minutes ON and 15 minutes OFF times. For a 22.2 V, 6.6 Ah Li-ion battery pack.

sufficiently accurate parameters estimates online, and within a single experimental run.

In the next section, the proposed online APE strategy is employed for real-time parameters estimation of a 400 V, 6.6 Ah, Li-ion battery bank. The Li-ion battery bank is utilized to power an indirect field-oriented control based electric vehicle (EV) traction system prototype. The real-time estimated parameters are also validated against the offline results on a 400 V, 6.6 Ah Li-ion battery bank.

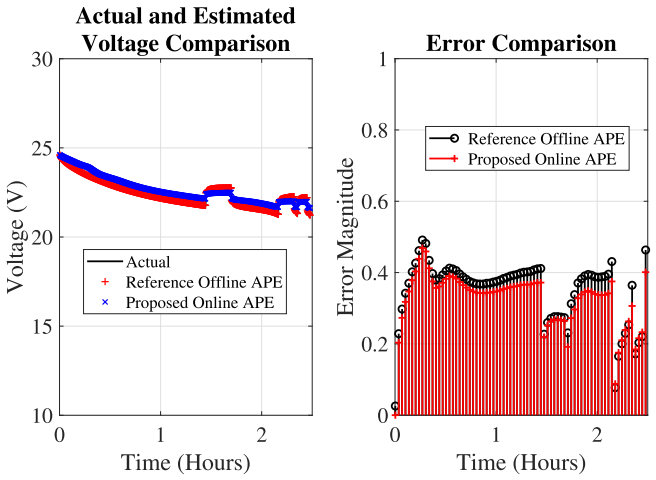

FIGURE 8. Terminal voltage estimation and absolute error $|e(t)|$ comparison for resistive load of 7.5 Ω with random time period. For a 22.2 V, 6.6 Ah Li-ion battery pack.

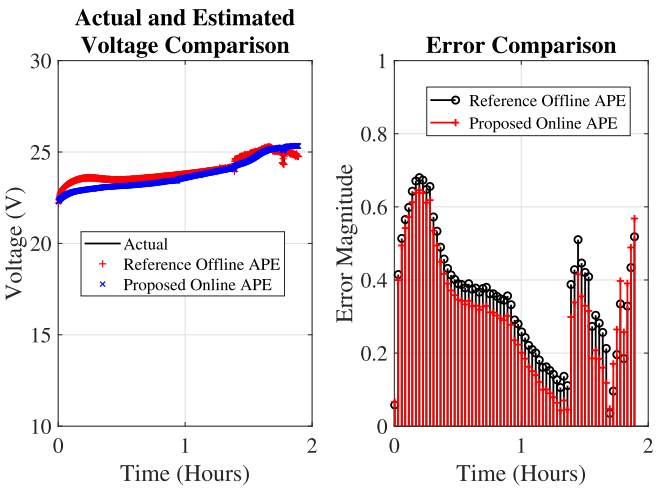

FIGURE 9. Terminal voltage estimation and absolute error $|e(t)|$ comparison while charging a 22.2 V, 6.6 Ah Li-Polymer battery pack.

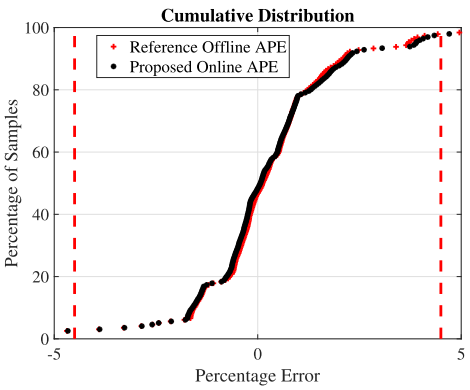

FIGURE 10. Cumulative distribution of terminal voltage estimation error for reference offline APE and proposed online APE under sixteen different discharging profiles, tested on 22.2 V, 6.6 Ah Lithium-ion battery packs. [No. of samples is in $O(10^7)$.].

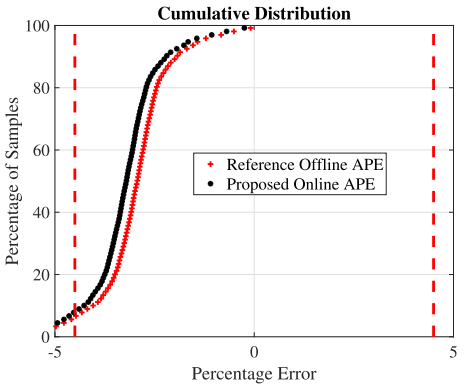

FIGURE 11. Cumulative distribution of terminal voltage estimation error for reference offline APE and proposed online APE techniques while charging sixteen individual 22.2 V, 6.6 Ah Lithium-ion battery packs with a constant 2.5 A current. [No. of samples is in $O(10^7)$.].

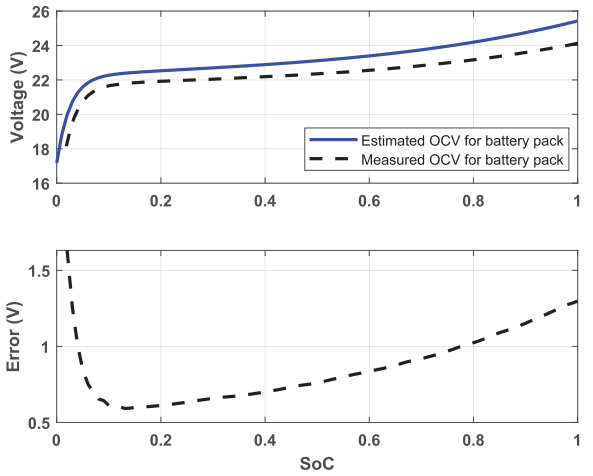

FIGURE 12. Comparison of measured and estimated open circuit voltage for a 22.2 V, 6.6 Ah Lithium-ion battery pack.

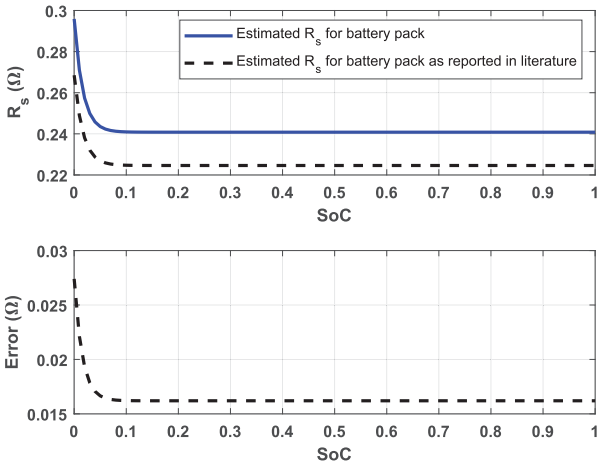

FIGURE 13. Comparison of estimated series resistance for a 22.2 V, 6.6 Ah Lithium-ion battery pack, with values available in the literature.

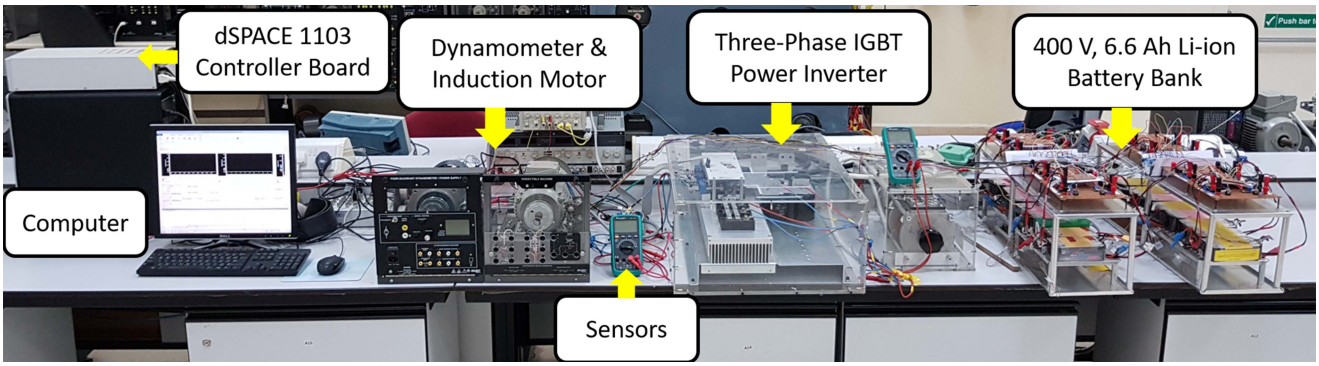

FIGURE 14. Li-ion battery bank powered EV traction system prototype [25].

TABLE 3 Experimental Results of a 400 V, 6.6 Ah Li-Ion Battery Bank Model Parameters Estimation Test

Parameter	Upper bound (r_{nu})	Lower bound (r_{nl})	λ_{x_n}	λ_{y_n}	Initial value	Estimated value (Real-time)	Estimated value (Offline)	Estimation error (%)
$\widehat{r}_1$	150	45	50	50	100	97.5	97.51	0.01
$\widehat{r}_2$	50	20	50	50	2000	35	35.01	0.03
$\widehat{r}_3$	–	–	–	–	–	356.865	357.236	0.1
$\widehat{r}_4$	7.5	1.5	50	50	100	4.5	5.2	13.4
$\widehat{r}_5$	20	2	50	50	230	11	11.01	0.1
$\widehat{r}_6$	50	25	50	50	400	37.5	37.55	0.13
$\widehat{r}_7$	1	0.1	50	50	180	0.6125	0.5643	8.54
$\widehat{r}_8$	50	10	50	50	1700	30	30.01	0.03
$\widehat{r}_9$	0.1	0.01	50	50	240	0.0568	0.069	17.68
$\widehat{r}_{10}$	10	1	70	50	3600	6.4074	6.262	2.32
$\widehat{r}_{11}$	200	100	50	50	9300	150	150	0
$\widehat{r}_{12}$	0.1	0.01	50	50	264	0.0694	0.0693	0.14
$\widehat{r}_{13}$	1000	500	60	55	50000	760.8586	760.882	0.003
$\widehat{r}_{14}$	15	5	70	50	1000	10.8367	10.845	0.07
$\widehat{r}_{15}$	800	500	80	50	50000	684.6064	684.626	0.16
$\widehat{r}_{16}$	7000	5000	10	10	50000	5998.5	6000	0.025
$\widehat{r}_{17}$	50	5	50	50	1000	27.507	27.514	0.025
$\widehat{r}_{18}$	5000	3000	10	20	50000	3666	3666.71	0.02
$\widehat{r}_{19}$	25	5	50	50	100	15	15.014	0.1
$\widehat{r}_{20}$	40	15	50	50	1200	27.505	27.514	0.033
$\widehat{r}_{21}$	–	–	–	–	–	5.01	5.428	7.7

VII. ONLINE PARAMETERS ESTIMATION OF A 400 V, 6.6 AH LITHIUM-POLYMER BATTERY BANK: POWERING A PROTOTYPE ELECTRIC VEHICLE TRACTION SYSTEM

The picture of a complete prototype EV traction testbench is shown in Fig. 14 [25]. The real-time adaptive parameters estimation of a 400 V, 6.6 Ah Li-ion battery bank is performed by running the proposed algorithm with all the required conditions described in section IV. The Li-ion battery bank powers an indirect field-oriented control based induction motor driven prototype EV traction system. The no-load operation of an induction motor draws around 0.2 amperes current and is used as the discharge current for the battery bank. The estimated Li-ion battery bank parameters using the proposed approach are presented in Table 3. Note that in Table 3, certain values related to parameters $\widehat{r}_3$ and $\widehat{r}_{21}$ are shown by dashes. This is because $\widehat{r}_3$ and $\widehat{r}_{21}$ disappear from the observer equations used in the proposed online APE strategy. However, these parameters are calculated in real-time using equations (33)–(34). The battery parameters estimated at no-load condition can be employed for SoC and SoH estimation, open circuit voltage and series resistance estimation, and fault detection in a battery management system during any loading condition of the prototype EV traction system. The effectiveness of the proposed online APE strategy is further quantified by comparing estimated parameters with the ones obtained through offline experimentation. For that purpose, the 400 V, 6.6 Ah Li-ion battery bank is discharged through a 384 Ω, 600 W resistive load. The battery bank discharge current and voltage profiles along with the estimated terminal voltage during the adaptation process are shown in Fig. 15, a zoomed view of the actual and estimated terminal voltages during the adaptation process, are shown in Fig. 16. The detailed procedure of the proposed online APE strategy has been described in Section III, and the results of estimated battery bank parameters are given in Table 3. The real-time estimated parameters of a 400 V, 6.6 Ah Li-ion battery bank model are quantified against the parameters obtained through offline mode. The estimation error in Table 3 shows the accuracy of real-time parameters. The accuracy of the online estimated parameters is assessed by analyzing the estimated terminal voltage us-

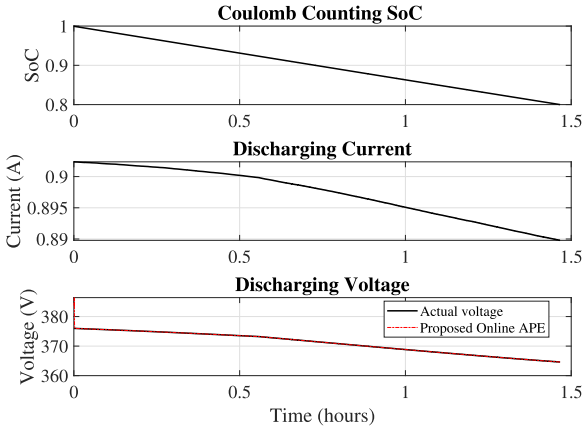

FIGURE 15. 400 V, 6.6 Ah Lithium-polymer battery bank discharging SoC, current, and voltage profiles during adaptation process.

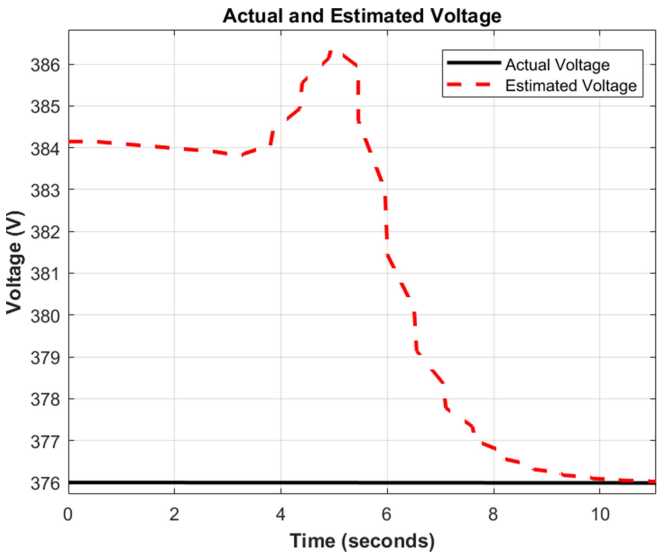

FIGURE 16. 400 V, 6.6 Ah Lithium-polymer battery bank discharging voltage profiles during adaptation process - zoomed version of last subplot in Fig. 15.

ing a fast periodic discharge profile through a resistive load rated at 230 Ω, 1000 W. The time period of the discharging profile is two minutes with 50% duty cycle. The real measured and estimated terminal voltages, using the parameters values estimated, is used to quantify the effectiveness of the proposed approach at the bank level. These details along with the terminal voltage estimation error are illustrated in Fig. 17. The terminal voltage estimation error in Fig. 17 is around 1% which proves the effectiveness of the proposed online APE strategy.

It is worth noting that the terminal voltage estimation error is seen to increase slightly towards the end in Fig. 17. This is because batteries are known to enter an unstable region when the battery SoC falls below a low value [24]. Further details about battery stability, are available in Section VIII-A. In this work there are limits to be satisfied by the SoC e.g. as in Theorem 2, $z(t) > \max\{\delta_1, \delta_2, \delta_3(t)\}$, and there are limits and conditions to be satisfied by the current. However, in our tests we do not pick any particular current profile. We also do not check that the battery SoC has not entered the unstable region [24] because this requires the parameters values - which we do not have access to in the beginning. However, the UAS based adaptive controller is able to handle such change in stability, and is a reason we use a UAS based strategy this work. This is also seen in all our results as the terminal voltage estimation error only experiences very small changes towards the end.

Also, please note that the UAS based technique used here is an observer. It is not used to control or actuate any device in this work. So the problems related to high control effort as a result of noise, which affect UAS, do not affect us. Because the observer simply executes on a computer; so, regardless of noise the algorithm can supply whatever control signal it mathematically needs. This is observed in the results presented as well, because no filtering is used with any of the sensor readings used. Also, the only measurements are current and voltage, and for the order of signals measured (max. 400 V, and few amperes) it is not hard to get reasonably priced high-quality sensors for current and voltage measurement which are less susceptible to noise.

The statistical analysis of terminal voltage estimation error is also performed. Note that the total number of samples collected in the estimation error array during the discharging test are 73,529. The mean, median, mode, and standard deviation of the error array for the proposed online APE strategy are -2.7754 V, -2.7828 V, -6.1766 V, and 1.3199 V respectively. Moreover, the histogram of the terminal voltage estimation error is shown Fig. 18. The statistical analysis of terminal voltage estimation error shows the effectiveness of the proposed APE strategy for real-time parameters estimation on the EV traction system prototype.

For further validation, we compare the bank level OCV and series resistance estimated using parameters estimated at the bank level as in Table 3, with the bank level OCV and series resistance calculated using the parameters estimated at the cell (Table 1) level. And also we compare the bank level OCV and series resistance estimated using the parameters estimated at the bank level, with the bank level OCV and series resistance computed based on measurements at the pack level. This can be done because the battery pack rated at 22.2 V is made of 6 cells in series, each rated at 3.7 V. However upon fully charging, we have observed that the battery pack achieves a voltage of around 24 V i.e. each cell achieves a voltage of around 4 V. So multiplying the cell level voltage 6 times gives us the pack voltage. Further, the battery bank is made of 16 packs in series so the bank level OCV and series resistance can be computed by multiplying the cell level OCV and series resistance each by 6×16. Similarly the bank level OCV and series resistance can be computed by multiplying the pack level OCV and series resistance each by 6. The OCV comparison results are shown in Fig. 19. The black dashed curve in the topmost subplot in Fig. 19 shows the estimated bank OCV using parameters estimated at the

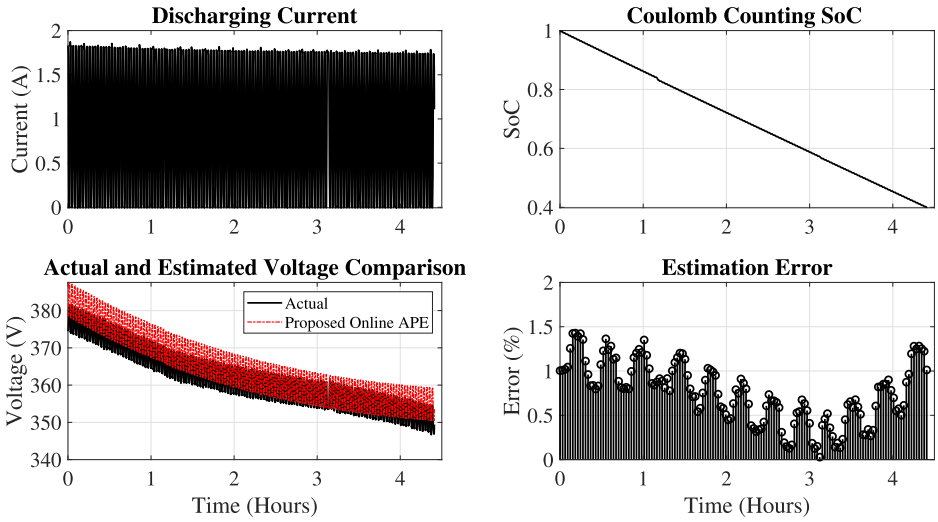

FIGURE 17. Terminal voltage estimation using the estimated parameters for a 400 V 6.6Ah Li-ion battery bank, and absolute error $|e(t)|$ comparison. A resistive load of 230 Ω, 1000 W is supplied with the following switching times: 1 minutes ON and 1 minute OFF.

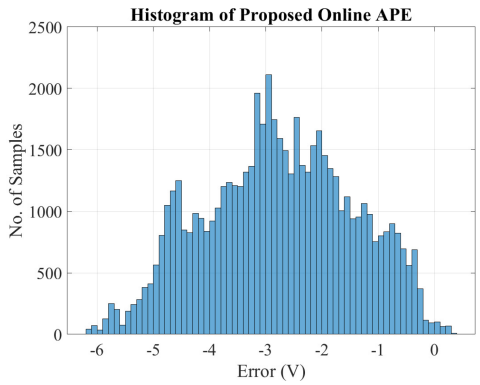

FIGURE 18. Histogram of terminal voltage estimation error for the proposed online APE strategy with the discharge profile shown in Fig. 17, on a 400 V, 6.6 Ah Li-ion battery bank.

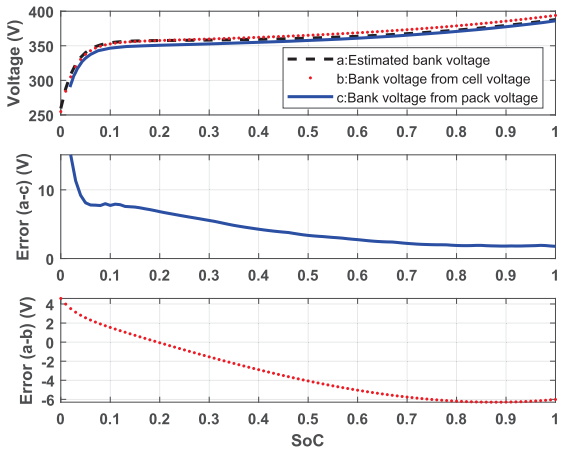

FIGURE 19. Comparison of open circuit voltage estimation performance for a 400 V 6.6Ah Li-ion battery bank.

bank level. The blue curve shows six times the measured OCV of one battery pack. And the red dotted curve shows the 96 times the cell OCV calculated using the paramters estimated at the cell level by [1], which were also rigorously verified in [1] against measurements. The middle and bottom subplots show the corresponding errors. As seen, the error in estimating bank OCV compared to the one computed from a pack level measurement is below 5 V (i.e. 1.3%) for 0.5 <SoC< 1. The maximum error is observed for SoC under 0.1 which is around 15 V (i.e. 3.9%). Also the maximum peak-to-peak error in estimating bank OCV compared to the one computed from a cell level estimate is around 10 V (i.e. 2.6%).

Similar plots for series resistance comparisons and the respective errors are shown in Fig. 20. As seen from the plots, the estimated bank level series resistance constructed from the pack level, has an error of only 1.157Ω compared to the series resistance directly estimated at the bank level, for SoC $>$ 0.1. For SoC $<$ 0.1 the error between the series resistance directly

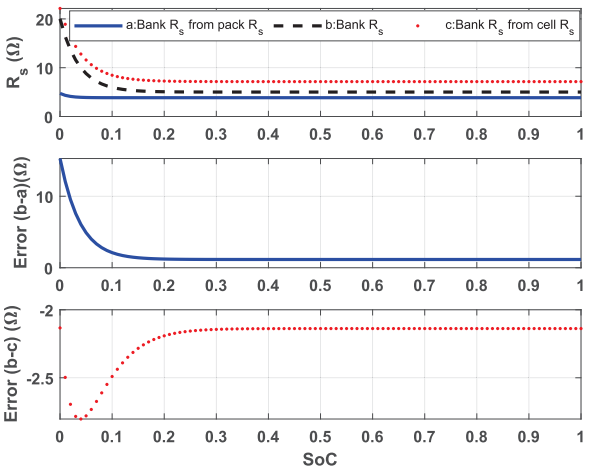

FIGURE 20. Comparison of series resistance estimation performance for a 400 V 6.6Ah Li-ion battery bank.

estimated at the bank level and the one computed from the pack level, increases. This may be because only one pack level estimate is considered and multiplied six times to get the bank level estimate. However, there may be differences between packs. In contrast, regardless of SoC, the the estimated bank level series resistance constructed from the cell level has an error of around 2 to 3Ω compared to the series resistance directly estimated at the bank level. So even though there may be cell level or pack level variability in series resistance, the ability to estimate them online in-runtime at any level, still has the ability to give sufficiently accurate results for SoC > 0.1. And, having access to the estimates at the cell and pack level, and having the ability to estimate them for any cell/pack may help compensate for cell level and pack level variability in the future - when creating bank level estimates.

VIII. DISCUSSION

A. LI-ION BATTERY STABILITY

It may be intuitive to think of stability for physical systems. But stability of equilibrium points of a system of differential equations - can be analyzed for any set of differential equations, regardless of whether such equations represent physical objects/behavior or not. For example, a thermal runaway may be attributed to a change in the stability of the differential equations governing the thermal dynamics [30], [31].

While less obvious, the sudden and near instantaneous drop in terminal voltage of a battery at the end of its runtime is attributed to a change in stability of the equations governing the electrical dynamics. This is shown, and used in [24], [32], [33], [34]. This can be understood by considering the battery terminal voltage equation in (6). The first term on the R.H.S. of (6) is the open circuit EMF, which is non-zero and bounded (even when the battery is at the end of its discharge cycle i.e. runtime). The last term consists of a product of the discharge current and the series resistance. Both of which are bounded in reality, and the latter is very small. All the terms themselves are positive, and x_1 is nearly constant throughout the life of the battery and diminishes marginally at the end of the runtime. But the actual terminal voltage is obtained by subtracting the voltage drops $x_2(t)$, $x_3(t)$, $i(t)x_4(t)$ from the open circuit EMF x_1. Also, in reality, at the end of the runtime of a battery, the current decreases because the battery is unable to maintain the current supply. So, the only way for the terminal voltage to drop to zero near instantaneously, without the current $i(t)$ increasing, is if the voltage drops x_2, x_3 increase very fast. Physically, this can be thought of as the parasitic voltage drops x_2, x_3 shown in figure 1 increasing very fast at the end of a discharge cycle, thus causing the terminal voltage to drop to zero very fast. The source of this can be traced back to the equilibrium points of (3)–(4) going from stable to unstable, as shown in [24], [32], [34]. This stability analysis (available in [24], [32], [34]) uses the equations of the equivalent circuit elements of the equivalent circuit model shown in figure 1, which are based on the extensive and rigorous experimental work in [1].

B. PERSISTENCE OF EXCITATION

When considering standard gradient based or least squares regression based parameter estimation approaches, equations of the form

$$y = Wa \tag{107}$$

are common. Where y is a vector of outputs, W is a matrix of signals/inputs, and a is a vector with parameters whose values need to be estimated. It is obvious that (107) is linear in the parameters a. For such parameters estimation problems as in (107), as indicated in well established literature [35], [36], one requires the input/signal matrix W to be persistently exciting. Specifically as per [36], a matrix W is persistently exciting if there exist positive constants α_1 and τ such that the below persistence of excitation (PE) condition is satisfied.

$$\int_t^{t+\tau} W^T W dr \geq \alpha_1 I, \ \forall \tau \geq 0 \tag{108}$$

Here I is an appropriately sized identity matrix. An equivalent but alternate statement of the PE condition [35] is, "the input signal has as many sinusoids as there are unknown parameters".

In fact [36] states that in the case of linear systems m sinusoids in the input signal can guarantee the estimation of upto $2m$ parameters. It is also stated in [36] that for nonlinear systems, not only is the requirement of the PE condition unclear, but also it is possible to estimate more than $2m$ parameters with an input containing m sinusoids.

At this juncture we would like to draw attention to the following facts. The output equation for terminal voltage (6), which is used in this work is of the form,

$$y = f(W, a). \tag{109}$$

Here y is the output terminal voltge, W represents the states x_1 through x_4 and the discharge current, a represents all the parameters which enter the state and output equations (1)–(6) non-linearly. The observer for estimating these parameters utilizes this exact same nonlinear structure in (16)–(21), and adds an input u to the estimator equations (18)–(20). Further, as defined in [23], and as seen in [26] the input used is a Nussbaum function of Mittag-Leffler type. By definition of a Nussbaum function in [23], such an input is required to oscillate rapidly, and the frequency of oscillation must keep varying. So given the varying frequency of the input Nussbaum function, and recalling the equivalent statements of the PE condition; we see that the requirement for having enough sinusoids injected into the system is easy to fulfill. Not only that, but because our parameters estimation problem is not-linear and of the type in (109), as mentioned above it may be possible to estimate the parameters with far fewer number of sinusoids being injected into the system compared to the number of parameters. Thus not imposing the PE condition explicitly, still allows us to obtain satisfactory results as reported in the paper.

It is also worth noting that there exists work on parameters estimation which does not explicitly impose the PE condition [37], and achieves reliable parameter estimates. And work

related to using the UAS based approach for parameters estimation exists, and has been rigorously verified in [2], [25], [38], [39].

C. SELECTION OF BOUNDS, CONFIDENCE LEVELS, AND INITIAL VALUES

1) FOR THE OPEN CIRCUIT EMF E_0

The open circuit EMF has the following form, $E_o(z) = -r_1 e^{-r_2 z} + r_3 + r_4 z - r_5 z^2 + r_6 z^3$. As the terminal voltage curve of a Li-ion battery is mostly flat for the SoC $z \in [0, 1]$ so the constant term r_3 is the most dominant one, and should have an order of magnitude close to the rated voltage of the battery. Also the exponential term only plays a noticeable role when $z \leq 10\%$, it is observed that r_2 is of the order of 10. The other constants r_1, r_4, r_5, r_6, as observed from the current work and [1], [2] are approximately one order of magnitude smaller than that of r_3. This provides a baseline for selecting the respective upper and lower bounds.

2) FOR RESISTANCES R_{ts}, R_{tl}, R_s

As reported in the literature, another characteristic of a Li-ion battery is almost no memory effect, i.e. the transient effects have some characteristic time constants. These are modeled by circuit elements R_{ts}, C_{ts} and R_{tl}, C_{tl}. The resistances R_{ts}, R_{tl} have the form $ae^{-bz} + c$, with $z \in [0, 1]$ being the SoC and $a, b, c > 0$. As the resistances R_{ts}, R_{tl} are only used in combination with the capacitances C_{ts}, C_{tl} to model transient characteristics, so these resistances R_{ts}, R_{tl} should not load the battery. This immediately provides that the values of a, c must be small i.e. usually of the order of 0.1 or 0.01. Also, for SoC approximately $\geq 10\%$ the values of the resistances R_{ts}, R_{tl} are constant at c and they increase a little for SoC $< 10\%$. This also gives that $a > c$, and b must be large enough to make the effects of the exponent term gradually disappear for $z > 0.1$. And the rate of change of R_{ts}, R_{tl} between c to a for SoC $\leq 10\%$ is controlled by b. Since these resistances model transient characteristics, and are independent of whether the characteristics are for a battery cell/pack/bank the range of values for a, b, c for R_{ts}, R_{tl} are the same for a battery cell/pack/bank. So either the above discussion, or an established model of a Li-ion battery cell from the literature [1] can be used and the upper and lower bounds i.e. r_{nu}, r_{nl} of a, b, c can be selected by adding $\pm 10\%$ to the values available in the literature. Similar considerations also apply to the series resistance R_s. However if the value of c for R_s for a single cell is of the order of 0.01 then for a 6S pack using 6 such cells in series the value of c would now be of the order of 6×0.01 for the pack. Similarly if now 16 such battery packs were used in series to make a battery bank then the order of c would now be $16 \times 6 \times 0.01$ for the bank.

3) FOR CAPACITANCES C_{ts}, C_{tl}

Similar characteristics are observed for C_{ts}, C_{tl} too. The capacitances C_{ts}, C_{tl} have the form $-\bar{a}e^{-\bar{b}z} + \bar{c}$, with $z \in [0, 1]$ being the SoC and $\bar{a}, \bar{b}, \bar{c} > 0$. From the literature [1] it is observed that $\bar{a}, \bar{c}$ are usually of the order of 100 or 1000 with $\bar{b}$ being of the order of 10. Also, for SoC approximately $\geq 10\%$ the values of the capacitances C_{ts}, C_{tl} are constant at $\bar{c}$ and they decrease for SoC $< 10\%$. The literature [34] also shows that respective constants $\bar{a}, \bar{b}, \bar{c}$ for C_{ts}, C_{tl} have an order relation. The discussion in this paragraph, or an established model of a Li-ion battery cell from the literature [1] can be used and the upper and lower bounds i.e. r_{nu}, r_{nl} of $\bar{a}, \bar{b}, \bar{c}$ can be selected by adding $\pm 10\%$ to the values available in the literature. However, for the case of capacitances, there are some constraints that need to be satisfied by the upper and lower bounds i.e. r_{nu}, r_{nl} and their respective confidence levels $\lambda_{x_n}, \lambda_{y_n}$. These constraints (linear inequalities in $r_{nu}, r_{nl}, \lambda_{x_n}, \lambda_{y_n}$) are mentioned in the statement of Lemma 1, and are required for the convergence of the observer in this work. The constraints are not hard to fulfill, one must simply check if the upper and lower bounds and their respective confidence levels selected, satisfy these inequality constraints. If they do not, one may simply update the values of the upper/lower bounds/ their respective confidence levels until the inequalities are satisfied.

4) THE CONFIDENCE LEVELS $\lambda_{x_n}, \lambda_{y_n}$

The role of the confidence levels $\lambda_{x_n}, \lambda_{y_n}$ may be further understood by looking at (61). The quantities $\lambda_{x_n}, \lambda_{y_n}$ control the rate at which the estimated parameters values $\hat{r}_n$ settle. Very large values for $\lambda_{x_n}, \lambda_{y_n}$ may result in quick settlement but would not allow for the estimation error to influence the value of $\hat{r}_n$. Very small values of $\lambda_{x_n}, \lambda_{y_n}$ on the other hand may allow the error to keep driving the value of $\hat{r}_n$ so it does not settle. This may allow effects of noise that shows up in the measured terminal voltage and battery current to be reflected in the estimation error e, and further affect the convergence of $\hat{r}_n$. As observed in this work and in [2], values of $\lambda_{x_n}, \lambda_{y_n}$ in the order of 10 seems to provide good performance.

5) INITIAL GUESSES

Selecting initial guesses for the initial values of the parameters is also not challenging because the initial values can simply be selected to be a number within the range of the upper and lower bounds. The only conditions on initial conditions, which are required to be satisfied for convergence, are related to C_{ts}, C_{tl} and are given in Corollary 1. The conditions are that $\widehat{r}_{13}(t_0) > \widehat{r}_{15}(t_0) > 0, \widehat{r}_{14}(t_0) \geq -\alpha e^{\frac{\ln(a_{min^1})}{z_{\min}}}$ and $\widehat{r}_{16}(t_0) > \widehat{r}_{18}(t_0) > 0, \widehat{r}_{17}(t_0) \geq -\alpha e^{\frac{\ln(a_{min^2})}{z_{\min}}}$. Although these may look involved, they are not. This is because one can easily select initial values such that $\widehat{r}_{13}(t_0) > \widehat{r}_{15}(t_0) > 0$ and $\widehat{r}_{16}(t_0) > \widehat{r}_{18}(t_0) > 0$. Doing this makes the quantities within the logarithms negative, as shown in the proof for Corollary 1. Now α is any positive constant, and $z_{\min}$ is the minimum value that the SoC is expected to reach. If one has no idea of $z_{\min}$ one can pick the lowest allowable SoC e.g. 7% for $z_{\min}$. Or as obvious, simply picking very large numbers for $\widehat{r}_{14}(t_0), \widehat{r}_{17}(t_0)$ also results in satisfying the logarithm related constraints from

Lemma 1. It is also observed from our experimentation, that the proposed strategy is effectively able to estimate the parameters values even if all of the various conditions related to the initial guesses, confidence levels, and bounds are not always strictly met.

D. ITERATIVE REFINEMENT OF THE BOUNDS, CONFIDENCE LEVELS, AND INITIAL VALUES.

Iterative methods using a combination of optimization along with UAS-based approaches are available in the literature, to tune the upper, lower bounds, respective confidence levels, and initial values [4], [38]. This enables the setting of initial guesses for the upper, lower bounds, respective confidence levels, and initial values; based on which an optimization routine determines the updated values of the upper, lower bounds, respective confidence levels, and initial values for the next iteration of parameters estimation. The goal can be to minimize the terminal voltage estimation error as used in [4], [38].

IX. CONCLUSION

An online UAS-based effective method for estimating Li-ion battery model parameters has been presented in this paper. The applicability of the developed method has been rigorously verified at the battery cell, pack and bank levels. In contrast to the reference offline UAS-based Li-ion battery parameters estimation; the proposed technique does not require prior offline experimentation for open circuit voltage estimation, and also eliminates post-processing for series resistance estimation. Numerical simulations are performed at the cell level on a 4.1 V, 270 mAh Li-ion battery model. Experimental results are provided on a 22.2 V, 6.6 Ah Li-ion battery pack. Furthermore, the proposed online APE strategy is implemented for real time, online parameters estimation of a 400 V, 6.6 Ah Li-ion battery bank; powering an indirect field-oriented induction motor driven EV traction system prototype. The real time results show parameters convergence within a few seconds and are validated against an offline test and fast periodic discharging battery bank voltage profile. The terminal voltage estimation error is around 1%, which proves the accuracy of the proposed online APE strategy for real time battery bank parameters estimation of an EV traction system.

APPENDIX

A. CONVERGENCE SPEED OF THE PROPOSED UAS-BASED METHOD

The parameter $k(t)$, adaptive gain $N(k(t))$, control input $u(t)$, and voltage estimation error $e(t)$ are shown in Fig. 21 during a 4.1 V Li-ion battery model parameters estimation process. The adaptive gain $N(k(t))$ settles to a steady state value in less than 150 samples, which implies $k(t) \to k_\infty$ by definition of Nussbaum function from equation (29)–(31). From equation (29), this further implies $\dot{k}(t) \to 0$, or $e(t) \to 0$ as $t \to t_c$, where t_c denotes the convergence time. Since, the sampling time of the proposed algorithm is set to 0.01 seconds, which

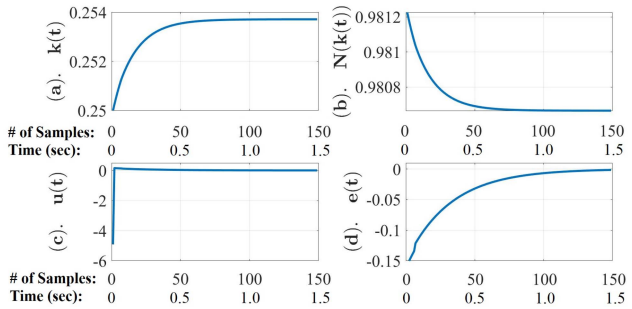

FIGURE 21. (a) Parameter $k(t)$, (b) adaptive gain $N(k(t))$, (c) control input $u(t)$, and (d) voltage estimation error $e(t)$ during a 4.1 V Li-ion battery model parameters estimation process.

indicates $t_c = 0.01 \times 150 = 1.5$ seconds. Therefore, irrespective of any traction system driving cycle/dynamic condition, the proposed strategy does not need to run for the entire driving cycle, rather it is run for a few seconds and enables self-update of battery parameters in run-time for battery management systems (BMS) and real-time electric vehicle (EV) applications.

In Fig. 22, the convergence of all battery parameters $\widehat{r}_1, \widehat{r}_2, \ldots, \widehat{r}_{21}$ is shown during the adaptive estimation process for a 4.1 V Li-ion battery. Note that the parameters $\widehat{r}_1, \widehat{r}_2, \ldots, \widehat{r}_{21}$ are normalized in Fig. 22 for clearly observing convergence. Many of the traces of the 21 battery parameters overlap in Fig. 22, and show convergence in under 0.25 seconds, but it can also be clearly seen that all the parameters $\widehat{r}_1, \widehat{r}_2, \ldots, \widehat{r}_{21}$ achieve convergence in less than 150 samples or 1.5 seconds.

Recently, a Trust Region Optimization (TRO) based Least-Squares method has been introduced in [13] to address the high computation time and slow convergence issues of the conventional Least-Squares method for battery parameters estimation. The work in [13] also presents the computation time of TRO-based Least-Squares method under various experiments, where the lowest computation time reported is 46 seconds. Emphasizing that the conventional Least-Squares method has significantly higher computation time with poor convergence compared to TRO-based Least-Squares method. Further, in our previous work [4], we significantly reduced the computation time of optimization-based methods by employing an adaptive strategy to fine-tune the search space interval required by the optimization method. In Table 4, we compare the computation/execution time of the proposed UAS-based scheme with TRO-based Least-Squares method, optimization-based methods, and two-stage adaptive scheme & optimization-based methods.

It is worth noting that the computation time of TRO-based Least-Squares method (an improved version of conventional Least-Squares method) it almost 30 times more than the proposed UAS-based approach for battery parameters estimation. The lower computation time shows the suitability of the proposed UAS-based approach for real-time battery parameters estimation in online or electric vehicle

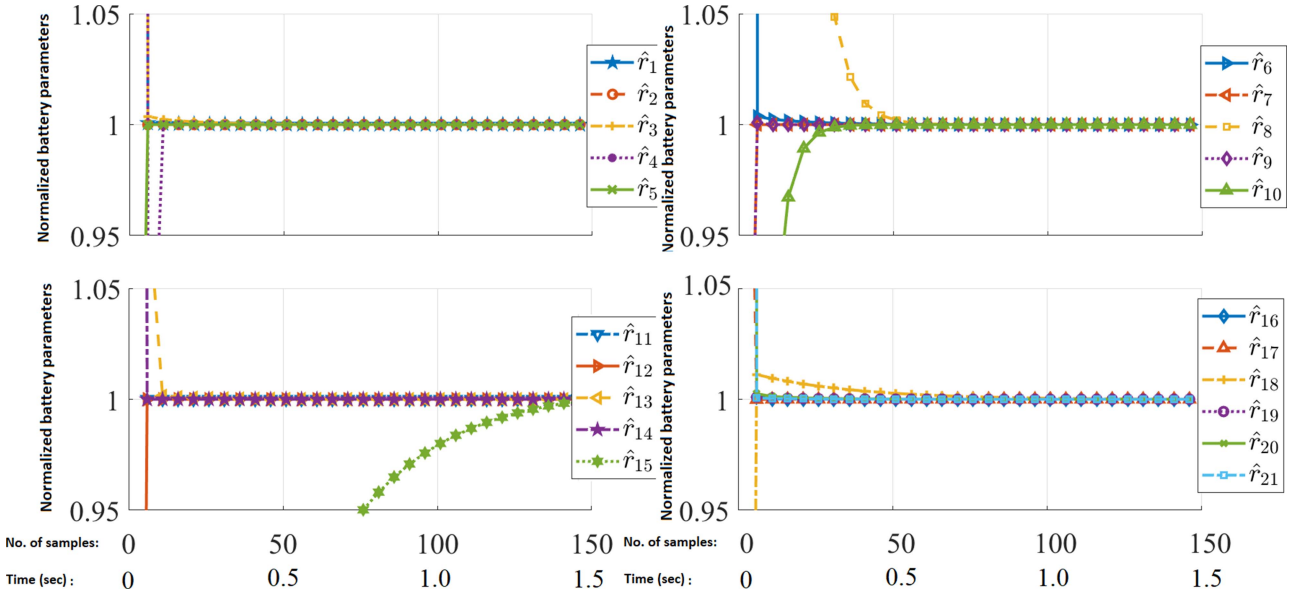

FIGURE 22. Parameters $\hat{r}_1, \hat{r}_2, \ldots, \hat{r}_{21}$ convergence during the adaptive estimation process for a 4.1 V Li-ion battery.

TABLE 4 Computation Time Comparison of the Proposed UAS-Based Scheme With TRO-Based Least-Squares Method, Optimization-Based Methods, and Two-Stage Adaptive Scheme & Optimization-Based Methods

Methods	Computation Time (seconds)
Particle Swarm Optimization (PSO)	34,200
Fmincon optimization	1,500
Hybrid (PSO-fmincon) optimization	39,780
Two-stage: Adaptive scheme & PSO	5,640
Two-stage: Adaptive scheme & fmincon	1,300
Two-stage: Adaptive scheme & Hybrid optimization	10,620
TRO-based Least Squares method	46
Proposed UAS-based approach	**1.5**

applications. The proposed strategy if run for a few seconds, may enable self-update of the battery parameters in run-time for battery management systems (BMSs), and may thus find use in real-time / electric vehicle (EV) applications.

Compared to methods like the extended Kalman filter (EKF) or the H-infinity filter which are shown to estimate terminal voltage in around 25 s at the cell level [40], the parameters and voltage estimation convergence time via the proposed method is 1.5 s at the 4.1 V cell level, and 10 s at the bank 400 V bank level. These are seen in Figs. 16, 21, and 22. A simple recursive least squares (RLS) procedure usually also ignores state dynamics and is only used for estimating the values of constants. It is also not robust to noise, and for avoiding such problems, state estimators like the EKF are used in the literature. As shown above the proposed approach can converge faster than the EKF, with satisfactory results.

B. COMMON RESULTS FROM REAL ANALYSIS

Consider the following details from [28]. For any positive integer n, let the metric space E^n represent the n-dimensional Euclidean space.

Theorem 3: "Any closed bounded subset of E^n is compact."

Proof: See [28, Chapter 3, Section 5]. □

Proposition 1: "Let f and g be real valued functions on a metric space E. If f and g are continuous at a point p_0 in E, then so are the functions $f+g$, $f-g$, fg, and f/g, the last under the proviso that $g(p_0) \neq 0$".

Proof: See [28, Chapter 4, Section 3]. □

Corollary 3: "A continuous real-valued function on a non-empty compact metric space, attains a maximum at some point and also attains a minimum at some point."

Proof: See [28, Chapter 4, Section 4]. □

REFERENCES

[1] M. Chen and G. Rincon-Mora, "Accurate electrical battery model capable of predicting runtime and I-V performance," *IEEE Trans. Energy Convers.*, vol. 21, no. 2, pp. 504–511, Jun. 2006.

[2] D. Ali, S. Mukhopadhyay, H. Rehman, and A. Khurram, "UAS-based Li-ion battery model parameters estimation," *Control Eng. Pract.*, vol. 66, pp. 126–145, Sep. 2017.

[3] H. M. U. Butt, S. Mukhopadhyay, and H. Rehman, "A two stage, adaptive-optimized Li-ion battery parameters estimation strategy," in *Proc. 11th Int. Symp. Mechatronics Appl.*, 2018, pp. 1–7.

[4] H. M. Usman, S. Mukhopadhyay, and H. Rehman, "Universal adaptive stabilizer based optimization for Li-ion battery model parameters estimation: An experimental study," *IEEE Access*, vol. 6, pp. 49546–49562, 2018.

[5] Q. Wang, J. Kang, Z. Tan, and M. Luo, "An online method to simultaneously identify the parameters and estimate states for lithium ion batteries," *Electrochimica Acta*, vol. 289, pp. 376–388, 2018.

[6] L. Zhao, Z. Liu, and G. Ji, "Lithium-ion battery state of charge estimation with model parameters adaptation using H_∞ extended Kalman filter," *Control Eng. Pract.*, vol. 81, pp. 114–128, 2018.

[7] M. Hu, Y. Li, S. Li, C. Fu, D. Qin, and Z. Li, "Lithium-ion battery modeling and parameter identification based on fractional theory," *Energy*, vol. 165, pp. 153–163, 2018.

[8] H. Rahimi-Eichi, F. Baronti, and M.-Y. Chow, "Online adaptive parameter identification and state-of-charge coestimation for lithium-polymer battery cells," *IEEE Trans. Ind. Electron.*, vol. 61, no. 4, pp. 2053–2061, Apr. 2014.

[9] A. Hentunen, T. Lehmuspelto, and J. Suomela, "Time-domain parameter extraction method for thévenin-equivalent circuit battery models," *IEEE Trans. Energy Convers.*, vol. 29, no. 3, pp. 558–566, Sep. 2014.
[10] F. Guo, G. Hu, and R. Hong, "A parameter adaptive method with dead zone for state of charge and parameter estimation of lithium-ion batteries," *J. Power Sources*, vol. 402, pp. 174–182, 2018.
[11] M. Kwak, B. Lkhagvasuren, J. Park, and J.-H. You, "Parameter identification and SOC estimation of a battery under the hysteresis effect," *IEEE Trans. Ind. Electron.*, vol. 67, no. 11, pp. 9758–9767, Nov. 2020.
[12] K. Sarrafan, K. M. Muttaqi, and D. Sutanto, "Real-time estimation of model parameters and state-of-charge of Li-ion batteries in electric vehicles using a new mixed estimation model," *IEEE Trans. Ind. Appl.*, vol. 56, no. 5, pp. 5417–5428, Sep./Oct. 2020.
[13] K. Saleem, K. Mehran, and Z. Ali, "Online reduced complexity parameter estimation technique for equivalent circuit model of lithium-ion battery," *Electric Power Syst. Res.*, vol. 185, 2020, Art. no. 106356.
[14] D. Dvorak, T. Bäuml, A. Holzinger, and H. Popp, "A comprehensive algorithm for estimating lithium-ion battery parameters from measurements," *IEEE Trans. Sustain. Energy*, vol. 9, no. 2, pp. 771–779, Apr. 2018.
[15] Z. Song, H. Wang, J. Hou, H. F. Hofmann, and J. Sun, "Combined state and parameter estimation of lithium-ion battery with active current injection," *IEEE Trans. Power Electron.*, vol. 35, no. 4, pp. 4439–4447, Apr. 2020.
[16] H. Chun, J. Kim, J. Yu, and S. Han, "Real-time parameter estimation of an electrochemical lithium-ion battery model using a long short-term memory network," *IEEE Access*, vol. 8, pp. 81789–81799, 2020.
[17] V.-H. Duong, H. A. Bastawrous, K. Lim, K. W. See, P. Zhang, and S. X. Dou, "Online state of charge and model parameters estimation of the lifepo4 battery in electric vehicles using multiple adaptive forgetting factors recursive least-squares," *J. Power Sources*, vol. 296, pp. 215–224, 2015.
[18] I. Jarrraya, L. Degaa, N. Rizoug, M. H. Chabchoub, and H. Trabelsi, "Comparison study between hybrid nelder-mead particle swarm optimization and open circuit voltage-recursive least square for the battery parameters estimation," *J. Energy Storage*, vol. 50, 2022, Art. no. 104424.
[19] K. Fan, Y. Wan, and B. Jiang, "State-of-charge dependent equivalent circuit model identification for batteries using sparse Gaussian process regression," *J. Process Control*, vol. 112, pp. 1–11, 2022.
[20] M. Lenz, D. Jöst, F. Thiel, S. Pischinger, and D. U. Sauer, "Identification of load dependent cell voltage model parameters from sparse input data using the mixed integer distributed ant colony optimization solver," *J. Power Sources*, vol. 437, 2019, Art. no. 226880.
[21] X. Hua, C. Zhang, and G. Offer, "Finding a better fit for lithium ion batteries: A simple, novel, load dependent, modified equivalent circuit model and parameterization method," *J. Power Sources*, vol. 484, 2021, Art. no. 229117.
[22] M. D. Berliner et al., "Nonlinear identifiability analysis of the porous electrode theory model of lithium-ion batteries," *J. Electrochem. Soc.*, vol. 168, Sep. 2021, Art. no. 090546.
[23] A. Ilchmann, "Non-identifier-based high-gain adaptive control," *Lecture Notes in Control and Information Sciences*, vol. 189. Berlin, Germany: Springer-Verlag, 1993.
[24] S. Mukhopadhyay and F. Zhang, "A high-gain adaptive observer for detecting Li-ion battery terminal voltage collapse," *Automatica*, vol. 50, pp. 896–902, Mar. 2014.
[25] H. M. Usman, H. Rehman, and S. Mukhopadhyay, "Performance enhancement of electric vehicle traction system using FO-PI controller," *IET Elect. Syst. Transp.*, vol. 9, no. 4, pp. 206–214, 2019.
[26] Y. Li and Y. Chen, "When is a Mittag–Leffler function a Nussbaum function?," *Automatica*, vol. 45, no. 8, pp. 1957–1959, 2009.
[27] S. Mukhopadhyay, "Mittag-Leffler function, M-file, cmex DLL, and S-function - file exchange - MATLAB central." Accessed: Sep. 30, 2022. [Online]. Available: https://www.mathworks.com/matlabcentral/fileexchange/20731
[28] M. Rosenlicht, *Introduction to Analysis*. New York, NY, USA: Dover, 1986.
[29] E. Lavretsky and K. A. Wise, *Robust and Adaptive Control*. London, U.K.: Springer-London, 2013.
[30] M. Citarella, D. Suzzi, B. Brunnsteiner, P. Schiffbänker, G. Maier, and J. Schneider, "Computational modelling of thermal runaway propagation in lithium-ion battery systems," in *Proc. IEEE Transp. Electrific. Conf.*, 2019, pp. 1–4.
[31] M. Cibrario and J. Levine, "Saddle-node bifurcation control with application to thermal runaway of continuous stirred tank reactors," in *Proc. 30th IEEE Conf. Decis. Control*, 1991, vol. 2, pp. 1551–155.
[32] F. Zhang, Z. Shi, and S. Mukhopadhyay, "Robustness analysis for battery-supported cyber-physical systems," *ACM Trans. Embed. Comput. Syst.*, vol. 12, Apr. 2013, Art. no. 69.
[33] S. Mukhopadhyay and F. Zhang, "Adaptive detection of terminal voltage collapses for Li-ion batteries," in *Proc. IEEE 51st IEEE Conf. Decis. Control*, 2012, pp. 4799–4804.
[34] S. Mukhopadhyay, "Robust forward invariant sets for nonlinear systems," Ph.D. dissertation, Dept. Elect. Comput. Eng., Georgia Inst. Technol., Atlanta, GA, USA, 2014.
[35] S. Sastry, *Nonlinear Systems: Analysis, Stability, and Control*. Berlin, Germany: Springer, 1999.
[36] J.-J. E. Slotine and W. Li, *Applied Nonlinear Control*. Englewood Cliffs, NJ, USA: Prentice-Hall, 1991.
[37] A. Stanislav, B. Alexey, O. Romeo, and P. Anton, "Performance enhancement of parameter estimators via dynamic regressor extension and mixing," *IEEE Trans. Autom. Control*, vol. 62, no. 7, pp. 3546–3550, Jul. 2017.
[38] S. Mukhopadhyay, R. Dhaouadi, M. Takrouri, and R. Dogga, "Supercapacitor characterization using universal adaptive stabilization and optimization," *IEEE Open J. Ind. Electron. Soc.*, vol. 1, pp. 166–183, 2020.
[39] A. Taieb, S. Mukhopadhyay, and A. Al-Othman, "Adaptive estimation of PEMFC stack model parameters - An experimental verification," *Int. J. Hydrogen Energy*, 2022. [Online]. Available: https://www.sciencedirect.com/science/article/pii/S0360319922023497
[40] C. Chen, F. Sun, R. Xiong, and H. He, "A novel dual H infinity filters based battery parameter and state estimation approach for electric vehicles application," *Energy Procedia*, vol. 103, pp. 375–380, 2016.

SHAYOK MUKHOPADHYAY (Member, IEEE) received the B.E. degree in electrical engineering from the College of Engineering Pune, Savitribai Phule Pune University, Pune, India, in 2006, the M.Sc. degree in electrical engineering from Utah State University, Logan, UT, USA, in 2009, and the Ph.D. degree in electrical engineering from the Georgia Institute of Technology, Atlanta, GA, USA, in 2014. He has been with the Department of Electrical Engineering, American University of Sharjah, United Arab Emirates, since 2014, where he is currently an Associate Professor. His research interests include control systems, energy storage systems, and robotic path planning. He was the recipient of the Award for the Best Presentation in the Nonlinear Systems III Session from the American Control Conference 2014. He was a part of a five-person team that received the national category of the AI and Robotics for Good Award for developing an in-pipe inspection robot at UAE in 2017.

HAFIZ M. USMAN (Student Member, IEEE) received the B.Sc. degree in electrical engineering from the University of Engineering and Technology, Lahore, Pakistan, in 2016, and the M.Sc. degree in electrical engineering from the American University of Sharjah, United Arab Emirates, in 2019. He is currently working toward the Ph.D. degree in power and energy systems with the University of Waterloo, Waterloo, ON, Canada. He was a Research Assistant with the American University of Sharjah from 2017 to 2019. His research interests include Li-ion batteries, power electronics and electric drives, control systems, renewable energy, and power distribution systems.

HABIBUR REHMAN (Member, IEEE) received the B.Sc. degree in electrical engineering from the University of Engineering and Technology, Lahore, Pakistan, in 1990, and the M.S. and Ph.D. degrees in electrical engineering from The Ohio State University, Columbus, OH, USA, in 1995 and 2001, respectively. He has a wide experience in the areas of power electronics and motor drives in both industry and academia. From 1998 to 1999, he was a Design Engineer with Ecostar Electric Drive Systems and Ford Research Laboratory, where he was a Member of the Electric, Hybrid, and Fuel Cell Vehicle Development Programs. From 2001 to 2006, he was with the Department of Electrical Engineering, United Arab Emirates (UAE) University, Al Ain, UAE, as an Assistant Professor. In 2006, he joined the Department of Electrical Engineering, American University of Sharjah, UAE, where he is currently working as Professor. His research interests include the areas of power electronics and their application to power systems, adjustable-speed drives, and alternative energy vehicles. He was the recipient of the Best Teacher Award (2002–2003) from the College of Engineering, UAE University.